Supporting Information for

Statistical Characteristics of Energetic Electron Pitch Angle Distributions in the Van Allen Probe Era: 1. Butterfly Distributions with Flux Peaks at Preferred Pitch Angles

L. G. Ozeke[1], I. R. Mann[1], L. Olifer[1], S. G. Claudepierre[2], H. E. Spence[3], and D. N. Baker[4]

[1]Department of Physics, University of Alberta, Edmonton, Alberta, Canada

[2]Department of Atmospheric and Oceanic Sciences, University of California, Los Angeles, CA, USA

[3]Institute for the Study of Earth, Oceans, and Space, University of New Hampshire, Durham, New Hampshire, USA

[4]Laboratory for Atmospheric and Space Physics, University of Colorado Boulder, Boulder, Colorado, USA

Corresponding author: Louis Ozeke (lozeke@ualberta.ca)

Contents of this file

Figures S1 to S29

Introduction

Figure S1 shows the L* values derived at local pitch angles of 90º, 35º and 0º along the orbital path of Van Allen Probe A during three geomagnetic storms. These results illustrate that below L*~5 (derived at a local pitch angle of 90º) the L* values are in general not strong functions of pitch angle.

Figure S2 panels (a) and (b) show an example of symmetric PAD fits derived using even Legendre coefficients which have a greater magnitude than the consecutive odd coefficients. Panels (c) and (d) show an example of an asymmetric PAD fit derived from Legendre coefficients, where $|C_2|<|C_3|$ and $|C_6|<|C_7|$. These results illustrate how the asymmetry in the PAD fits can be quantified by comparing the magnitude of the consecutive even and odd Legendre coefficients to identify highly asymmetric PADs likely resulting from errors in the flux measurements.

Figure S3 shows how the dip size, *DS*, of the butterfly pitch angle distributions (PADs) change as a function of the flux integrated over all equatorial pitch angle look directions, $J(\alpha_{eq})$, at L*=3.5 ±0.25 and L*=4.5 ±0.25 during time intervals with Dst=-30 ±15 nT. Figures S4, S5, S6 and S7 also show similar results during Dst=-60 ±15 nT and Dst=0 ±15 nT time intervals at L*=3.0, 3.5, 4.0, 4.5 and 5.0 ±0.25. These results are a supplement to the Dst=-30 ±15 results at L*=3.0, 4.0 and 5.0 ±0.25 presented in the main paper shown in Figure 7. These supporting Figures are in the same format as the results shown in Figure 7 and show that even during different levels of geomagnetic activity the butterfly PAD dip size, *DS*, of electrons in the outer radiation belt is generally smaller at higher total flux values integrated over all equatorial look directions, $J(\alpha_{eq})$.

Figure S8 shows the correlation between the flux at ~35° and ~90° for both butterfly and non-butterfly PADs at L*=3.5 ±0.25 and L*=4.5 ±0.25 during time intervals with Dst=-30 ±15 nT. Figures S9, S10, S11 and S12 also show similar results during Dst=-60 ±15 nT and Dst=0 ±15 nT time intervals at L*=3.0, 3.5, 4.0, 4.5 and 5.0 ±0.25. These results are a supplement to the Dst=-30 ±15 nT at L*=3.0, 4.0 and 5.0 ±0.25 presented in the main paper shown in Figure 8. All these results are in the same format and show that the electron flux in the outer radiation belt at these equatorial pitch angles remains correlated at each level of geomagnetic activity, even as the flux intensity changes by up to 4 orders of magnitude.

Figure S13 shows the ratio between the flux at ~35° and ~90° for both butterfly and non-butterfly PADs at L*=3.5 ±0.25 and L*=4.5 ±0.25 during time intervals with Dst=-30 ±15 nT. Figures S14, S15, S16 and S17 also show similar results during Dst=-60 ±15 nT and Dst=0 ±15 nT time intervals at L*=3.0, 3.5, 4.0, 4.5 and 5.0 ±0.25. These results are a supplement to the Dst=-30 ±15 nT at L*=3.0, 4.0 and 5.0 ±0.25 presented in the main paper shown in Figure 9. All these results are in the same format and illustrate that the flux ratios change with L-shell and electron energy in the same way during each level of geomagnetic activity.

Figures S18, S19, S20, S21, S22 and S23 show the correlation between the flux at ~65° and ~90° for both butterfly and non-butterfly PADs, during intervals with Dst=-60 ±15 nT, Dst=-30 ±15 nT and Dst=0 ±15 nT at L*=3.0, 3.5, 4.0, 4.5 and 5.0 ±0.25. These results are a supplement to the results presented in the main paper shown in Figure 8 and are in the same format as the results presented in Figures 8 in the main paper, as well as Figures S12, S13, S14, S15 and S16, showing that the flux at equatorial pitch angles of ~65° and ~90° remains highly correlated during each level of geomagnetic activity, even as the flux intensity changes by up to 4 orders of magnitude.

Figures S24, S25, S26, S27, S28 and S29 show the ratio between the flux at ~65° and ~90° for both butterfly and non-butterfly PADs during intervals with Dst=-60 ±15 nT, Dst=-30 ±15 nT and Dst=0 ±15 nT at L*=3.0, 3.5, 4.0, 4.5 and 5.0 ±0.25. These results are a supplement to the Dst=-30 ±15 nT results presented in the main paper shown in Figure 9. All these results are in the same format and illustrate that the flux ratios change with L-shell and electron energy in the same way during different levels of geomagnetic activity.

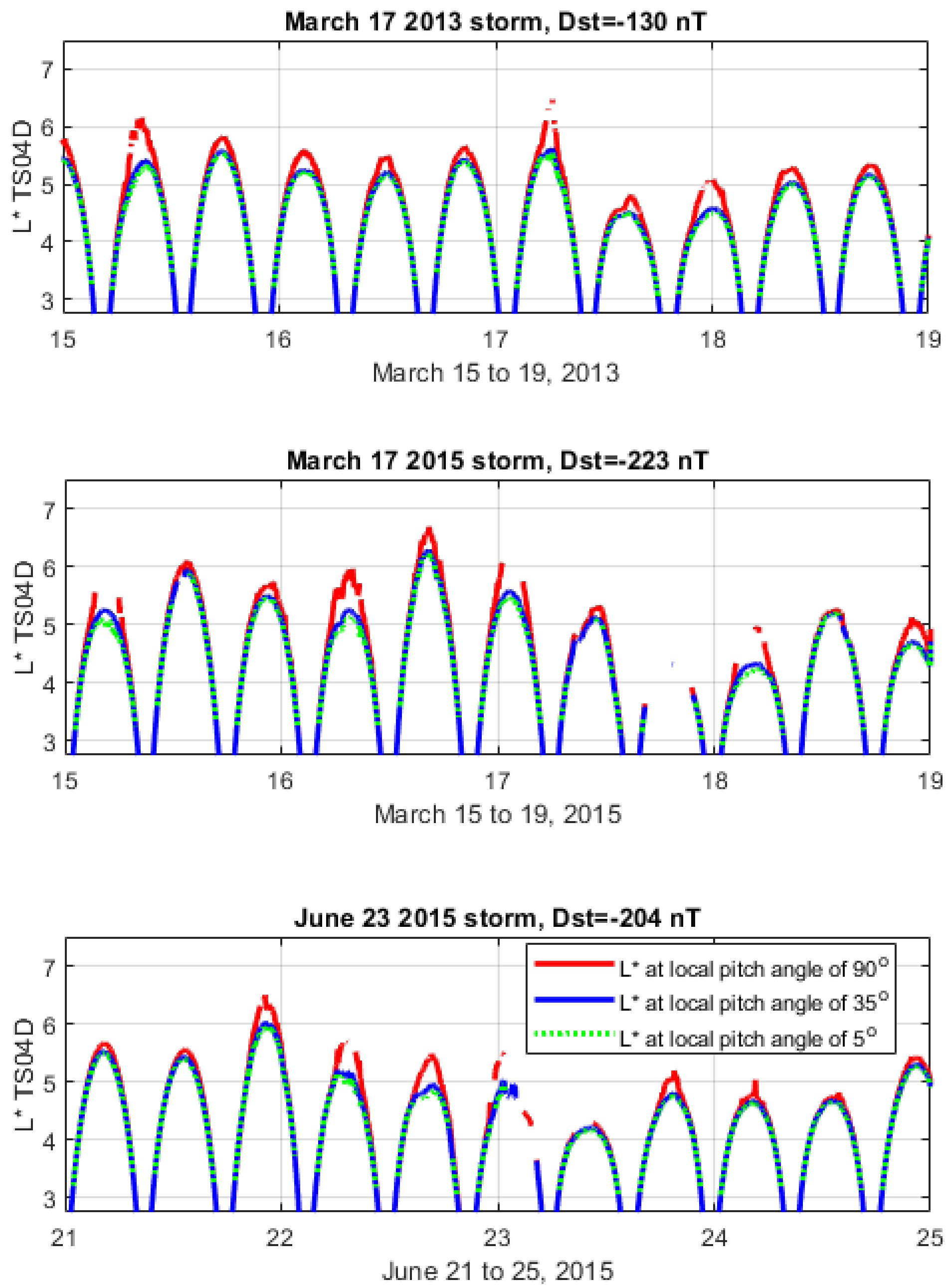

Figure S1. L* values derived at local pitch angles of 90º, 35º and 0º along the orbital path of Van Allen Probe A during three geomagnetic storms, illustrating that below L*~5 (derived at a local pitch angle of 90º) the L* values are in general not strong functions of pitch angle.

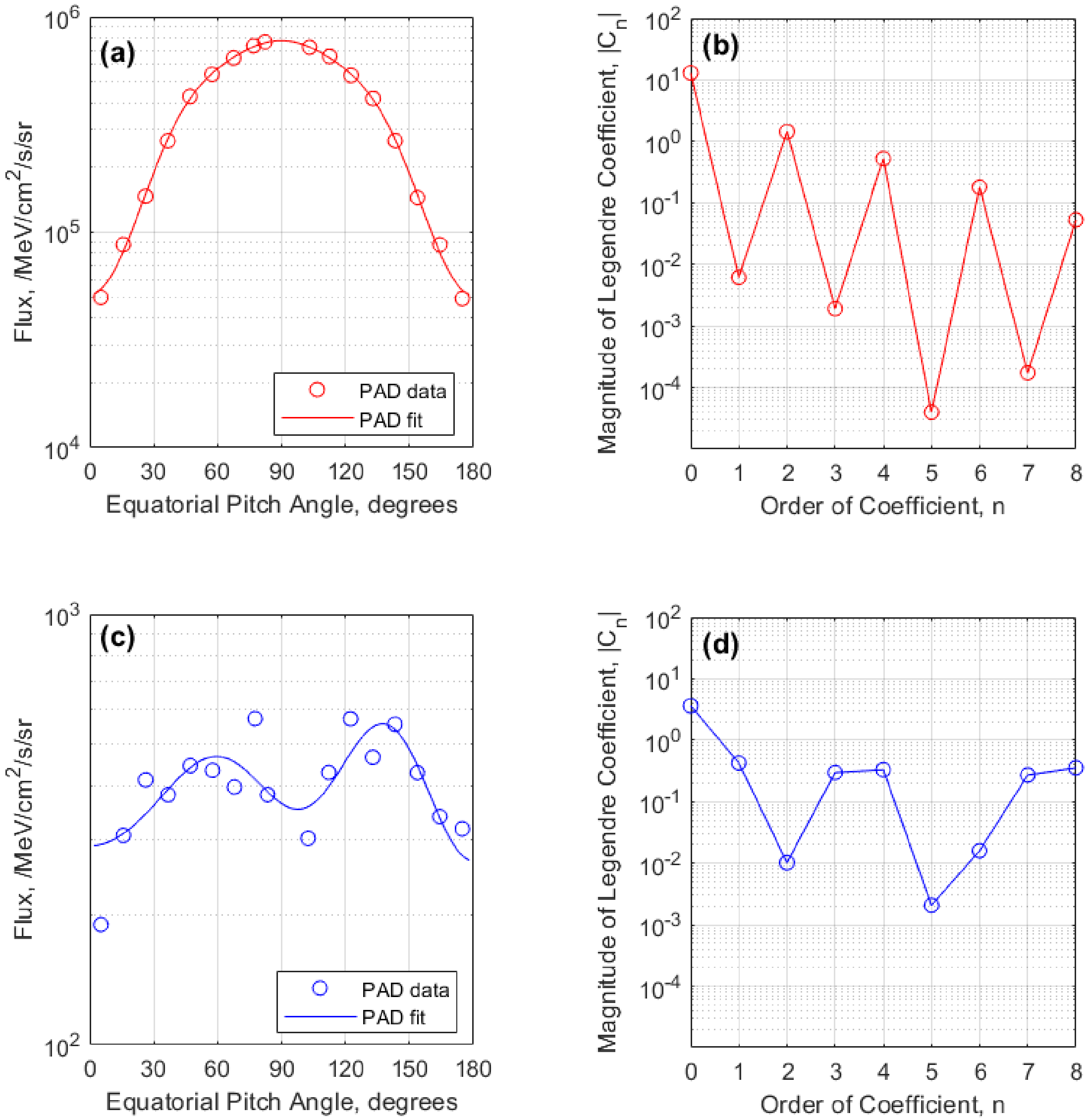

Figure S2. Panels (a) and (b) show an example of a symmetric PAD fit where the even Legendre polynomials are much greater than the consecutive odd coefficients. Panels (c) and (d) show an example of an asymmetric PAD fit where the even Legendre polynomials are not all greater than the consecutive odd coefficients. For example, $|C_2|<|C_3|$ and $|C_6|<|C_7|$.

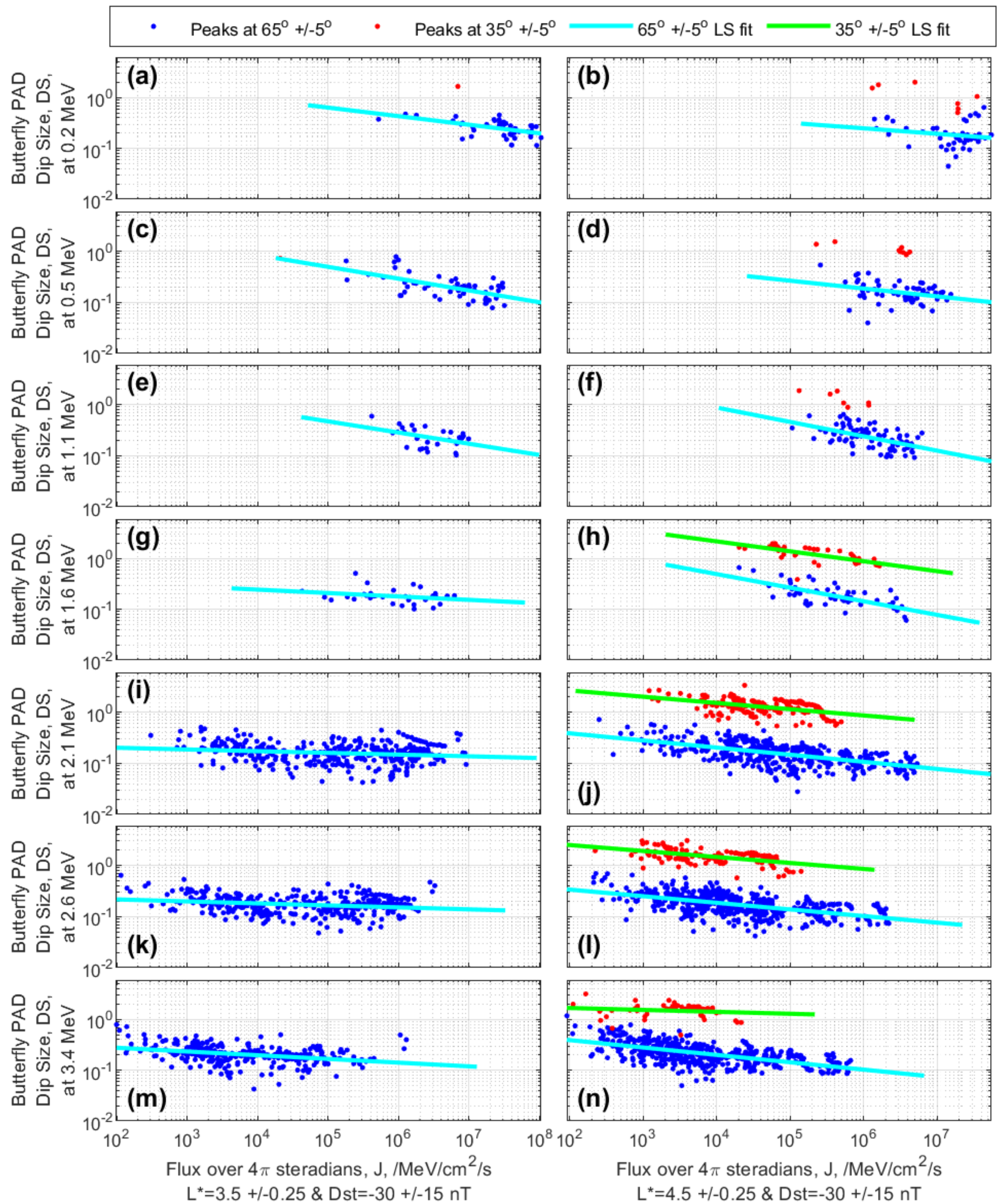

Figure S3. The dip size, *DS*, of butterfly PADs as a function of the flux integrated over all equatorial pitch angle look directions, $J(\alpha_{eq})$, at Dst=-30 ±15 nT for L*=3.5 ±0.25 and L*=4.5 ±0.25 in the same format as the results shown in Figure 7 in the main paper.

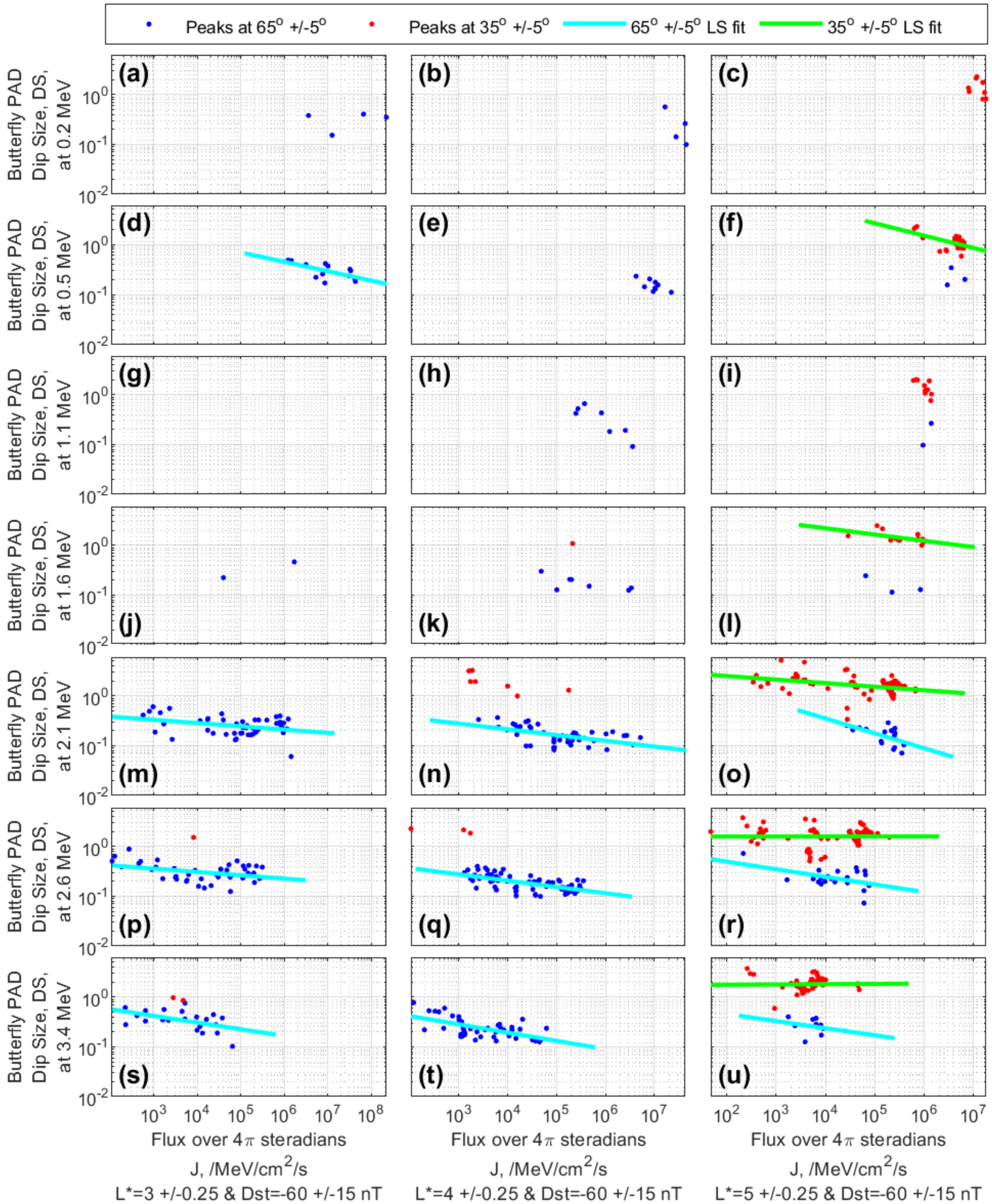

Figure S4. The dip size, *DS*, of butterfly PADs as a function of the flux integrated over all equatorial pitch angle look directions, $J(\alpha_{eq})$, for Dst=-60 ±15 nT, in the same format as the results shown in Figure 7 in the main paper.

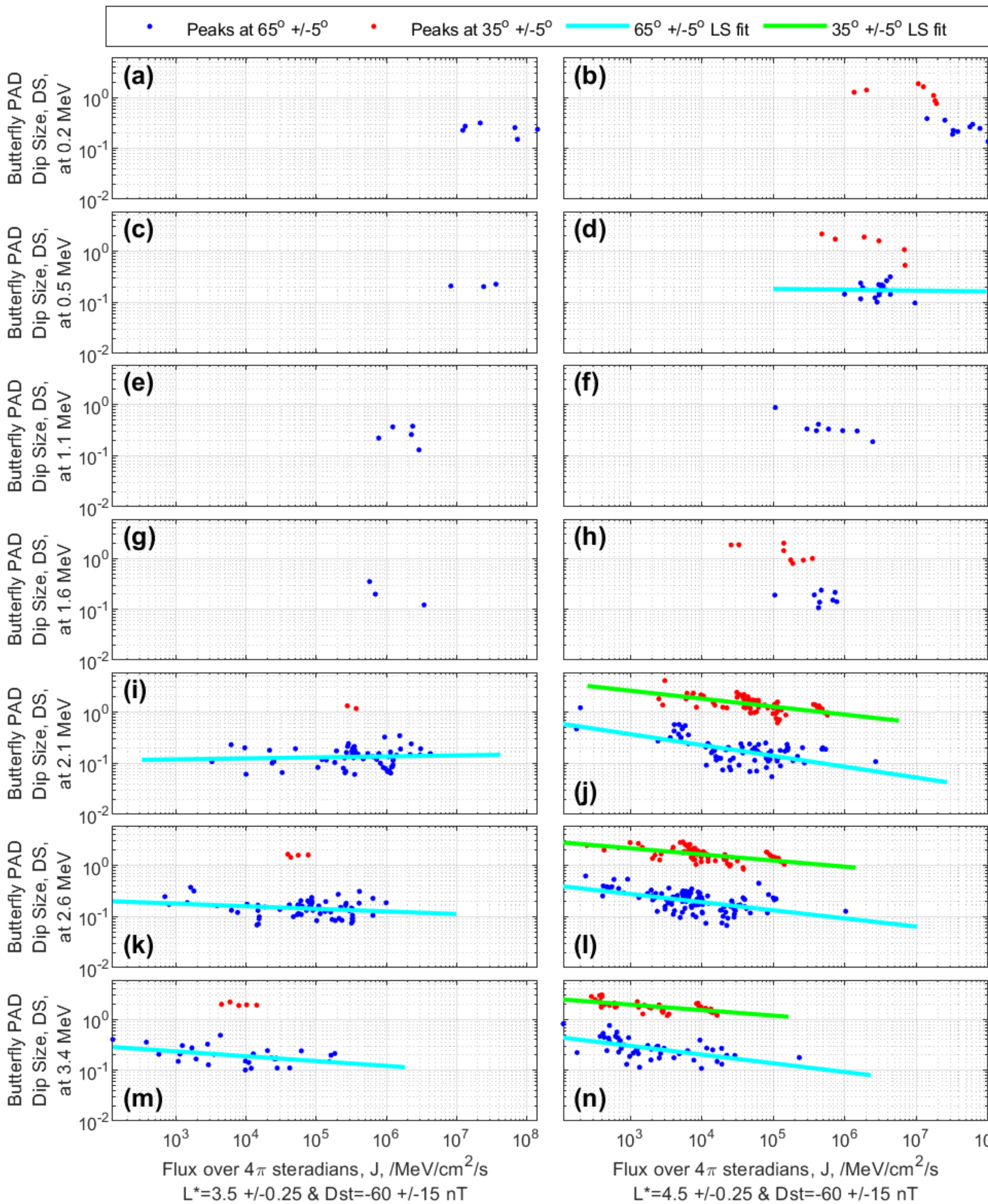

Figure S5. The dip size, *DS*, of butterfly PADs as a function of the flux integrated over all equatorial pitch angle look directions, $J(\alpha_{eq})$, at Dst=-60 ±15 nT for L*=3.5 ±0.25 and L*=4.5 ±0.25 in the same format as the results shown in Figure 7 in the main paper.

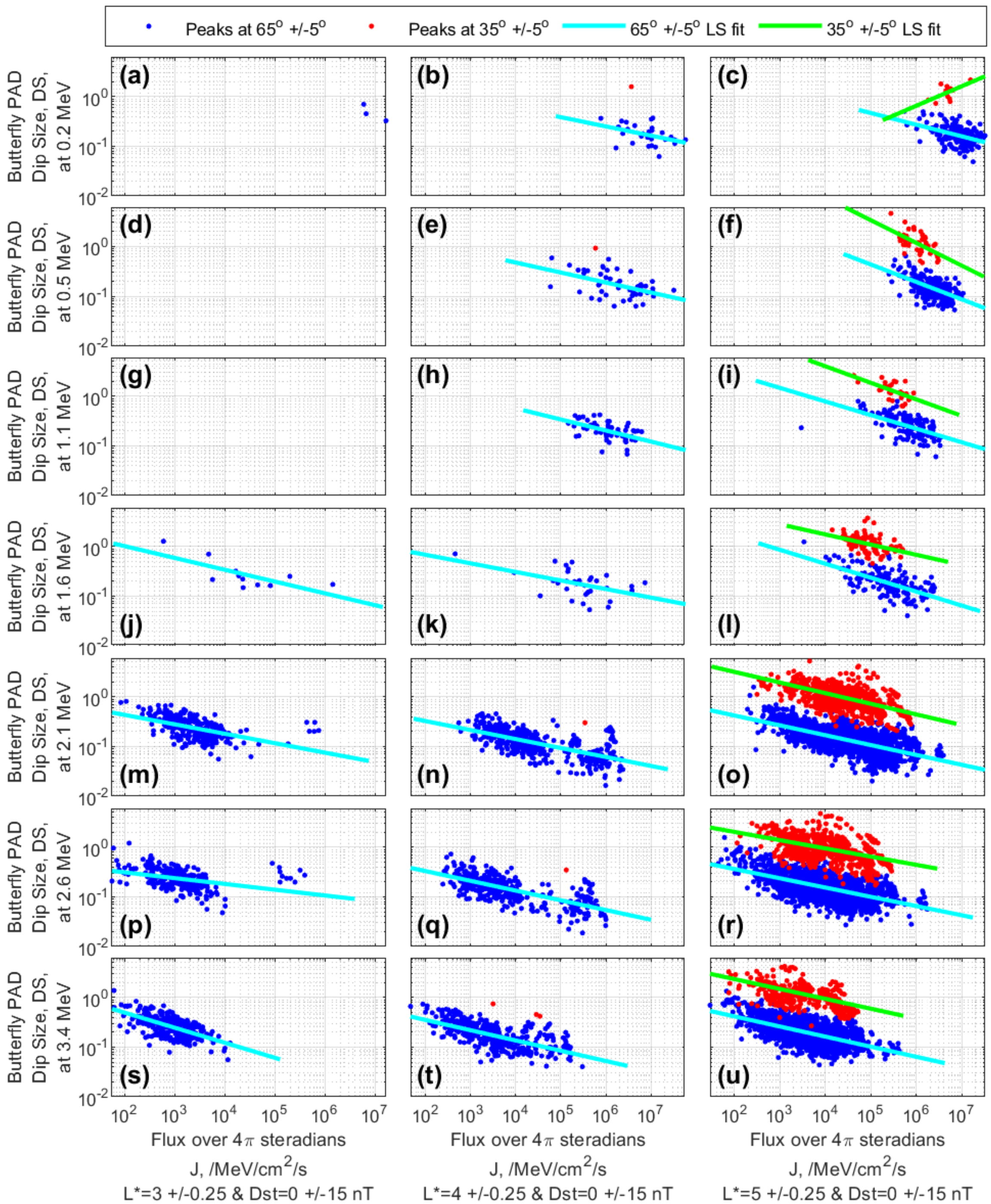

Figure S6. The dip size, *DS*, of butterfly PADs as a function of the flux integrated over all equatorial pitch angle look directions, $J(\alpha_{eq})$, for Dst=0 ±15 nT, in the same format as the results shown in Figure 7 in the main paper.

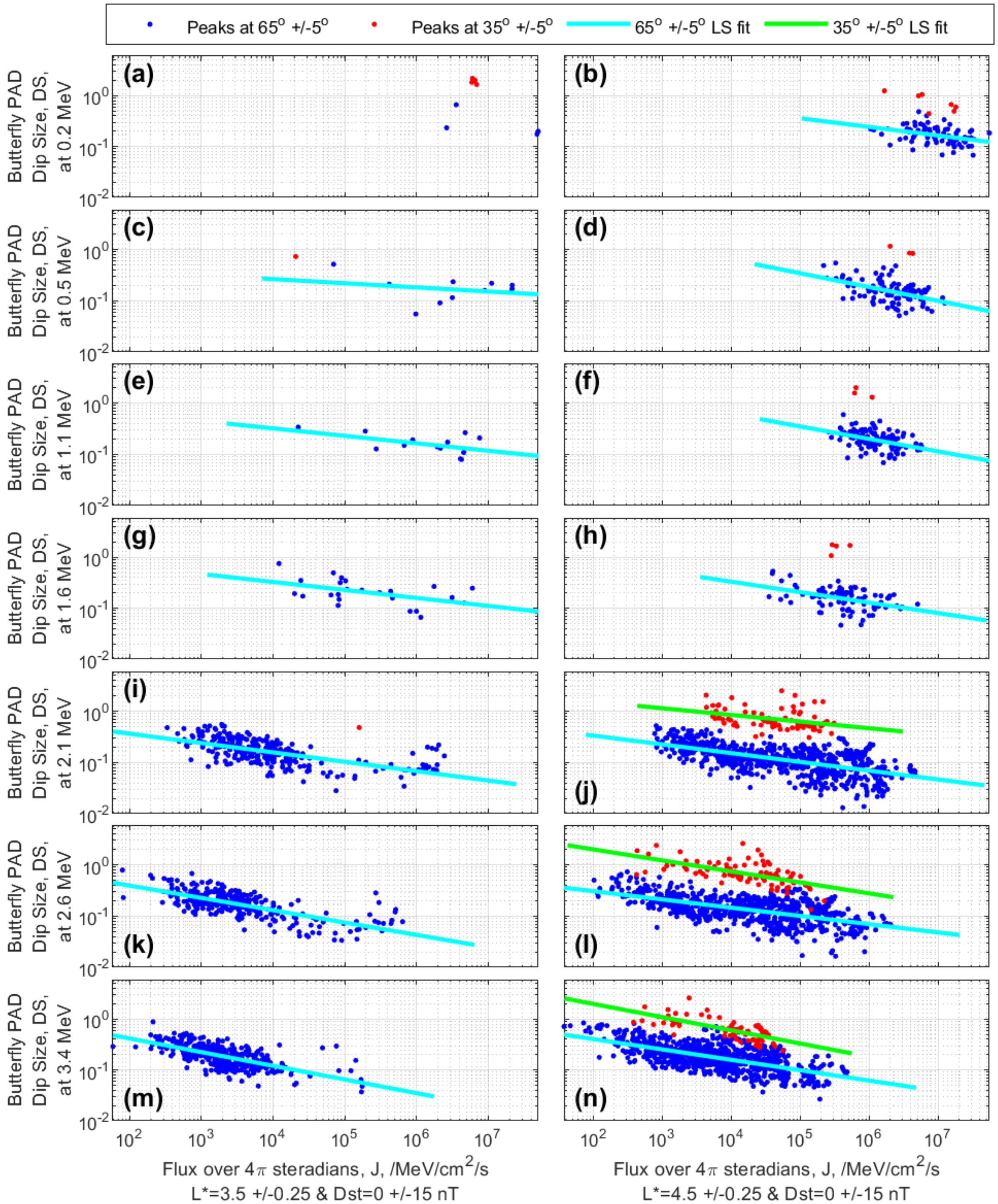

Figure S7. The dip size, *DS*, of butterfly PADs as a function of the flux integrated over all equatorial pitch angle look directions, $J(\alpha_{eq})$, at Dst=0 ±15 nT for L*=3.5 ±0.25 and L*=4.5 ±0.25 in the same format as the results shown in Figure 7 in the main paper.

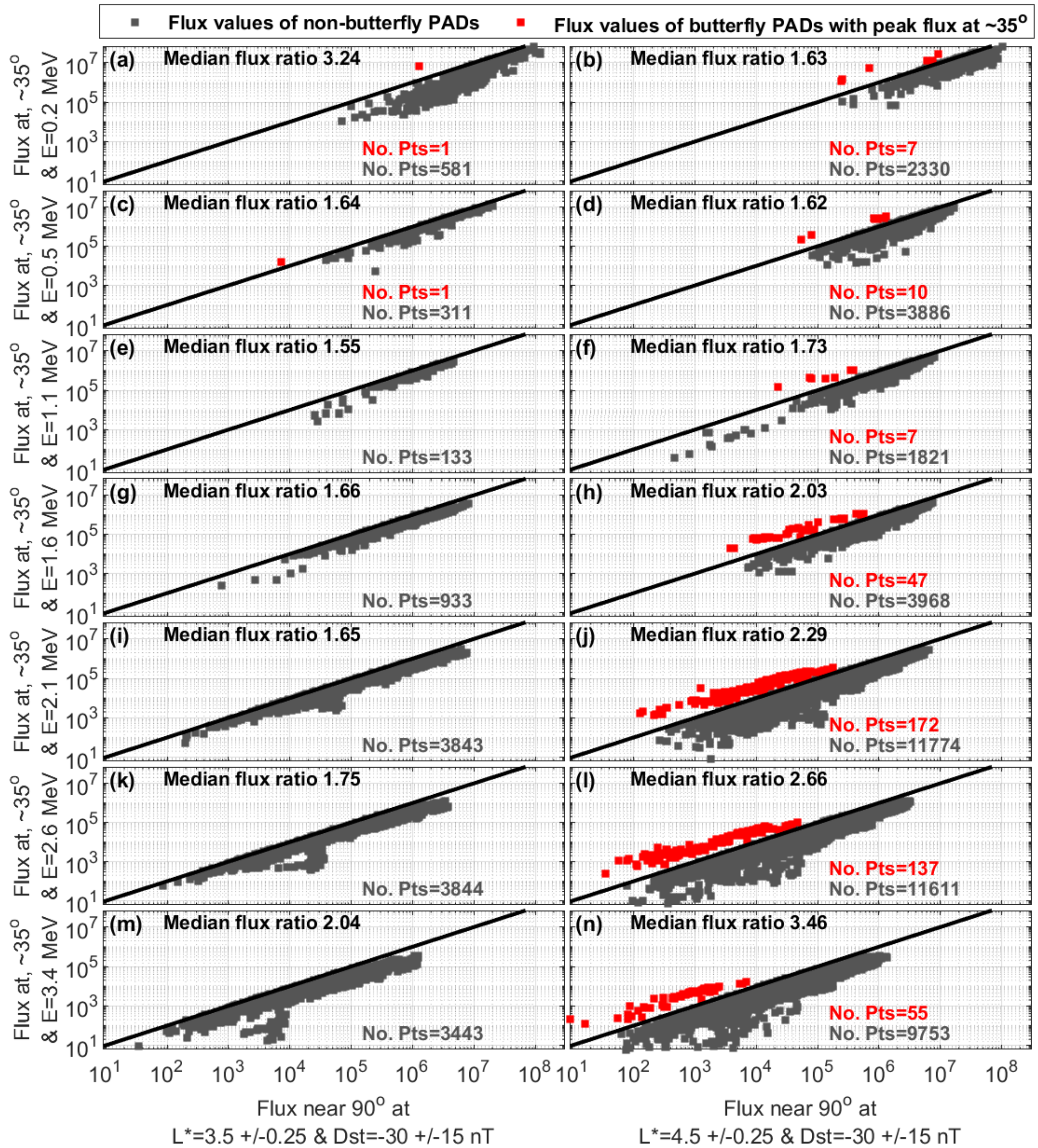

Figure S8. The red dots indicate results for butterfly PADs that have a peak flux at equatorial pitch angles of 35° ±5°. For these butterfly PADs each data point represents the flux near equatorial pitch angles of 35°, where the flux reaches a peak value, versus the flux near equatorial pitch angles of 90°, where the flux is at a local minimum. Similarly, the gray dots indicate results for non-butterfly PADs. For these non-butterfly PADs each data point represents the flux near an equatorial pitch angle of 90°, where the flux peaks, versus the flux at an equatorial pitch angle of 35°. Results shown here are for Dst=-30 ±15 nT at L*=3.5±0.25 and L*=4.5 ±0.25 in a similar format to the results presented in Figure 8 in the main paper.

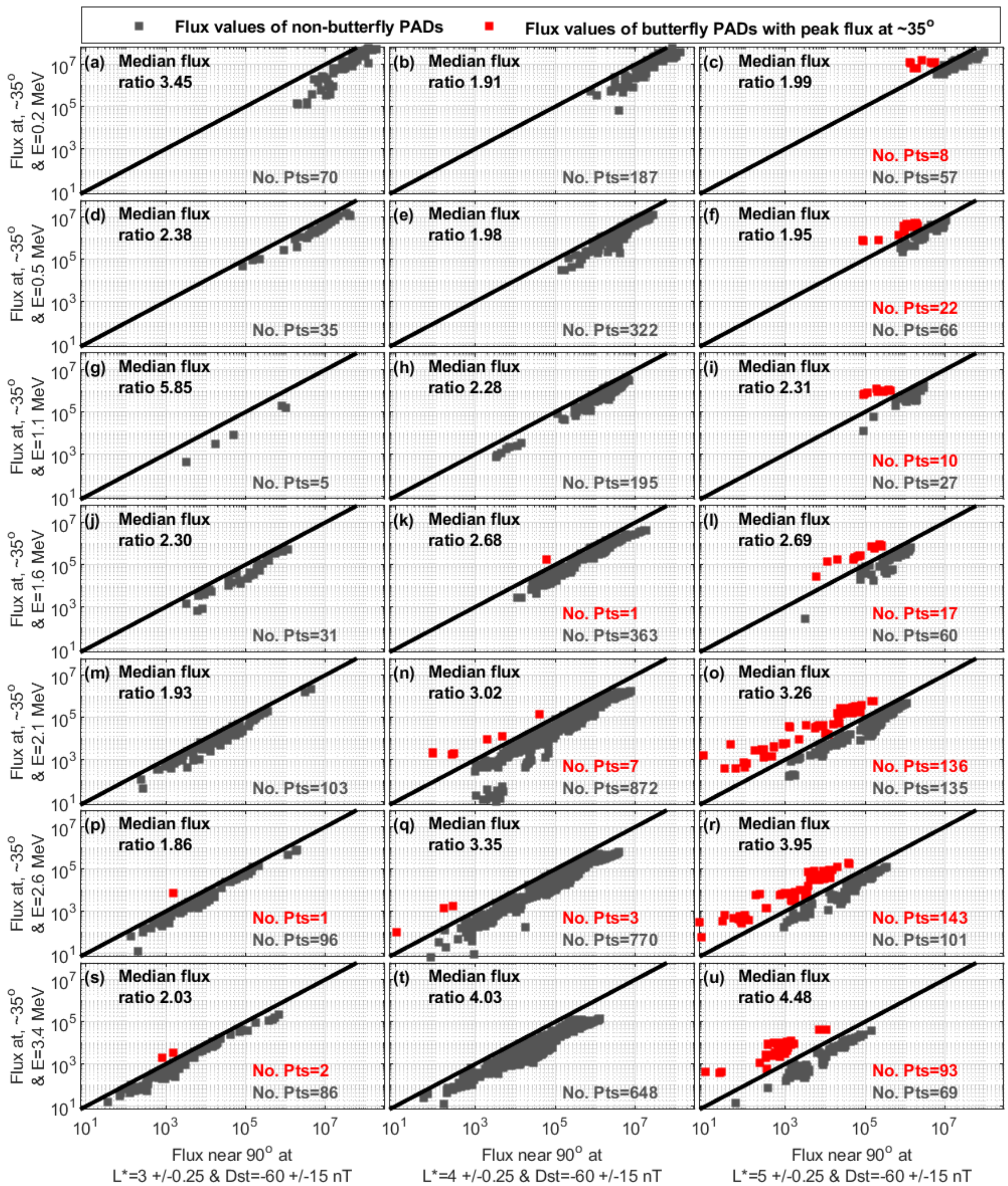

Figure S9. The red dots indicate results for butterfly PADs that have a peak flux at equatorial pitch angles of 35° ±5°. For these butterfly PADs each data point represents the flux near equatorial pitch angles of 35°, where the flux reaches a peak value, versus the flux near equatorial pitch angles of 90°, where the flux is at a local minimum. Similarly, the gray dots indicate results for non-butterfly PADs. For these non-butterfly PADs each data point represents the flux near an equatorial pitch angle of 90°, where the flux peaks, versus the flux at an equatorial pitch angle of 35°. Results shown here are for Dst=-60 ±15 nT, in a similar format to the results presented in Figure 8 in the main paper.

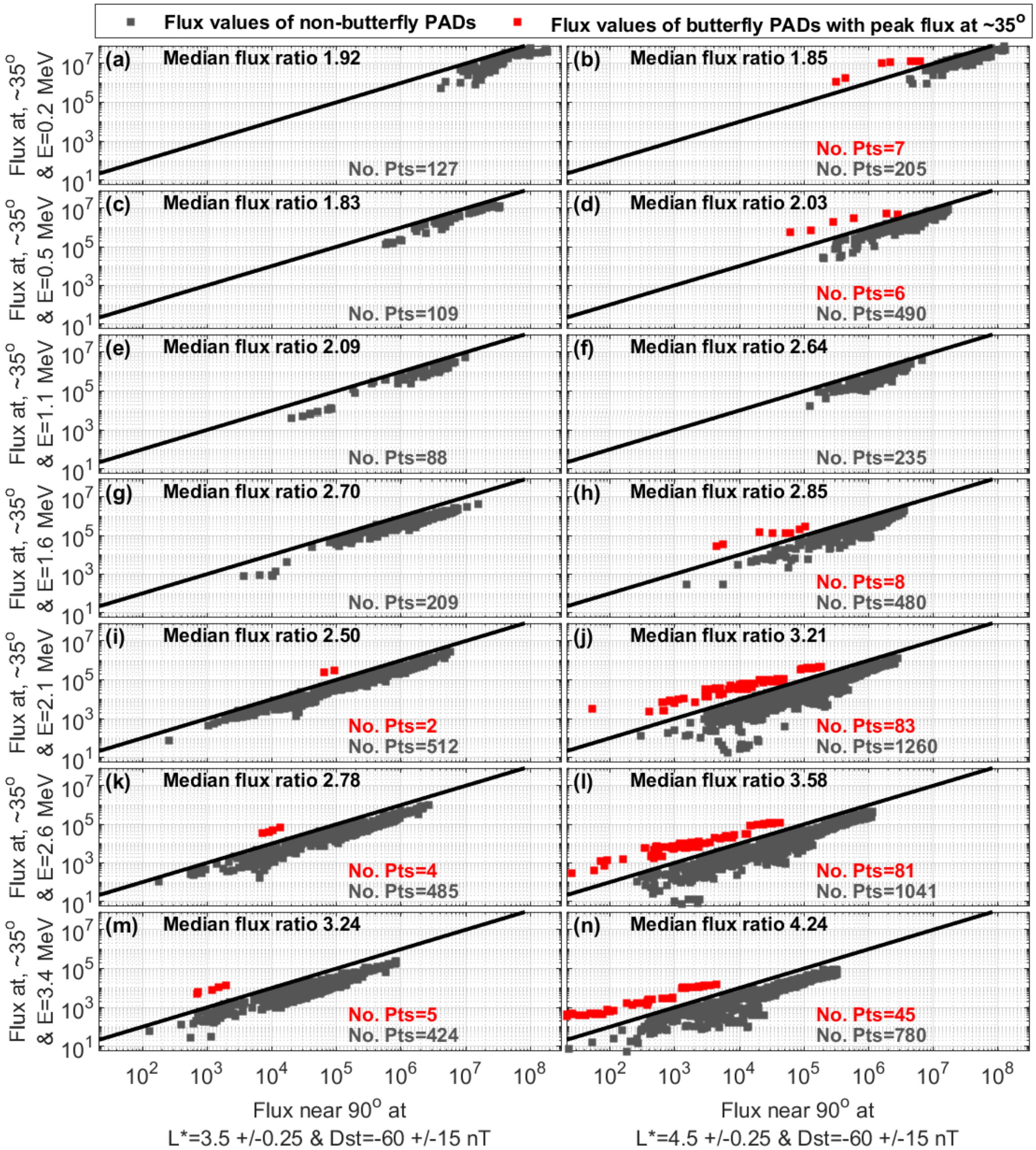

Figure S10. The red dots indicate results for butterfly PADs that have a peak flux at equatorial pitch angles of 35° ±5°. For these butterfly PADs each data point represents the flux near equatorial pitch angles of 35°, where the flux reaches a peak value, versus the flux near equatorial pitch angles of 90°, where the flux is at a local minimum. Similarly, the gray dots indicate results for non-butterfly PADs. For these non-butterfly PADs each data point represents the flux near an equatorial pitch angle of 90°, where the flux peaks, versus the flux at an equatorial pitch angle of 35°. Results shown here are for Dst=-60 ±15 nT at L*=3.5±0.25 and L*=4.5 ±0.25 in a similar format to the results presented in Figure 8 in the main paper.

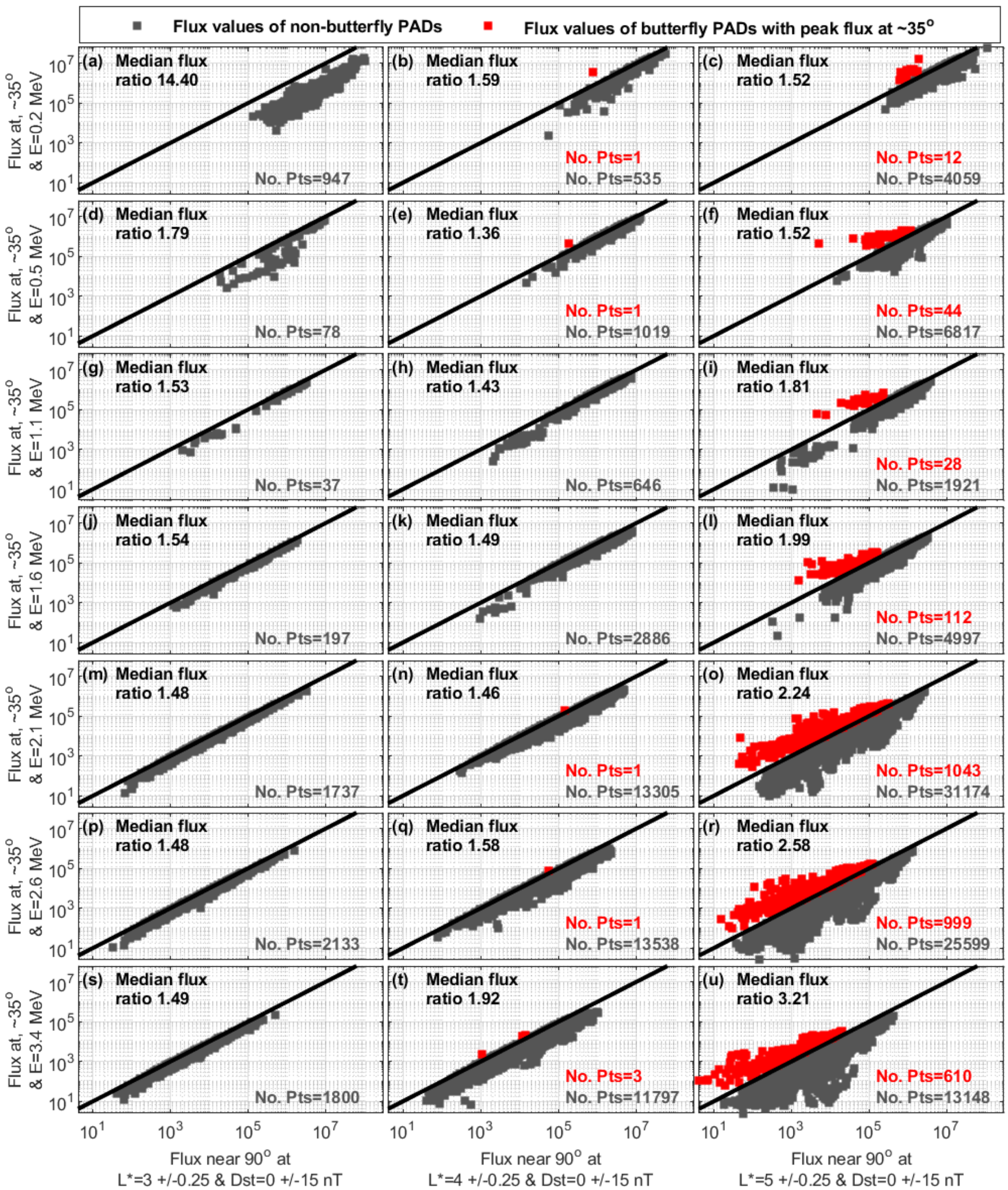

Figure S11. The red dots indicate results for butterfly PADs that have a peak flux at equatorial pitch angles of 35° ±5°. For these butterfly PADs each data point represents the flux near equatorial pitch angles of 35°, where the flux reaches a peak value, versus the flux near equatorial pitch angles of 90°, where the flux is at a local minimum. Similarly, the gray dots indicate results for non-butterfly PADs. For these non-butterfly PADs each data point represents the flux near an equatorial pitch angle of 90°, where the flux peaks, versus the flux at an equatorial pitch angle of 35°. Results shown here are for Dst=0 ±15 nT, in a similar format to the results presented in Figure 8 in the main paper.

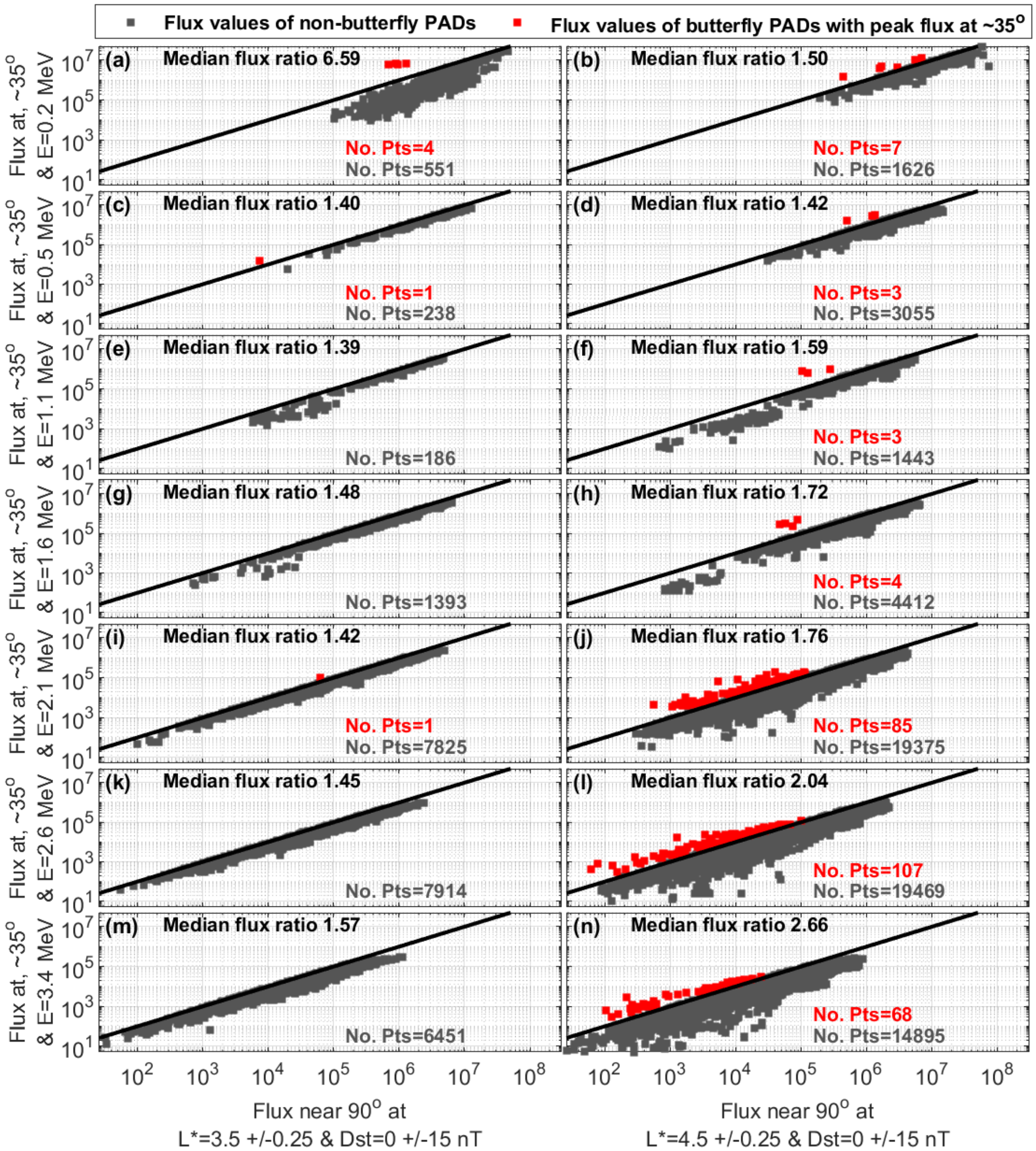

Figure S12. The red dots indicate results for butterfly PADs that have a peak flux at equatorial pitch angles of 35° ±5°. For these butterfly PADs each data point represents the flux near equatorial pitch angles of 35°, where the flux reaches a peak value, versus the flux near equatorial pitch angles of 90°, where the flux is at a local minimum. Similarly, the gray dots indicate results for non-butterfly PADs. For these non-butterfly PADs each data point represents the flux near an equatorial pitch angle of 90°, where the flux peaks, versus the flux at an equatorial pitch angle of 35°. Results shown here are for Dst=0 ±15 nT at L*=3.5±0.25 and L*=4.5 ±0.25 in a similar format to the results presented in Figure 8 in the main paper.

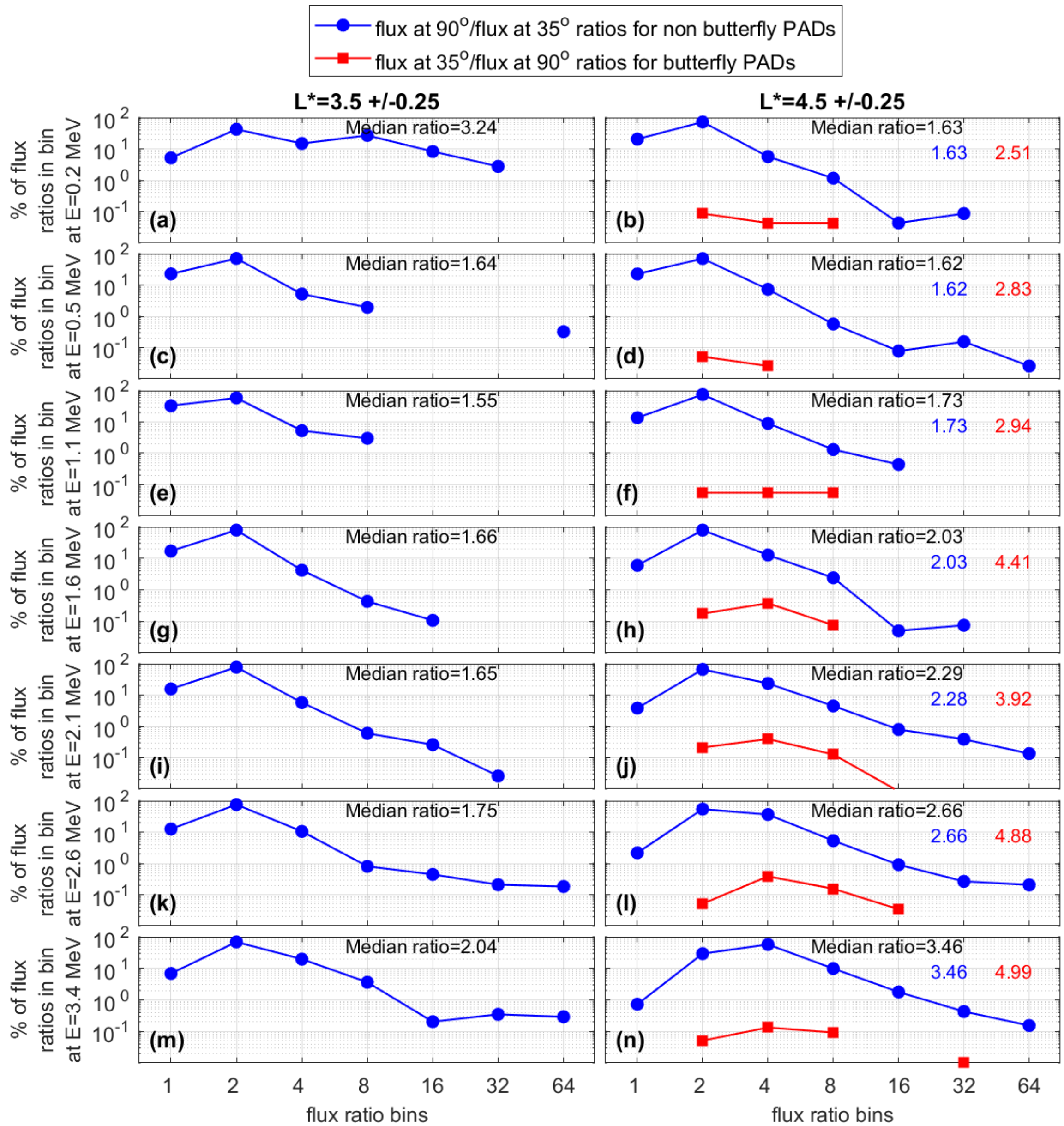

Figure S13. The curves indicate how the flux values at equatorial pitch angles of ~35° and ~90°differ. These results are for Dst=-30 nT ±15 nT at L*=3.5 ±0.25 and L*=4.5 ±0.25 in the same format as the results presented in Figure 9 in the main paper.

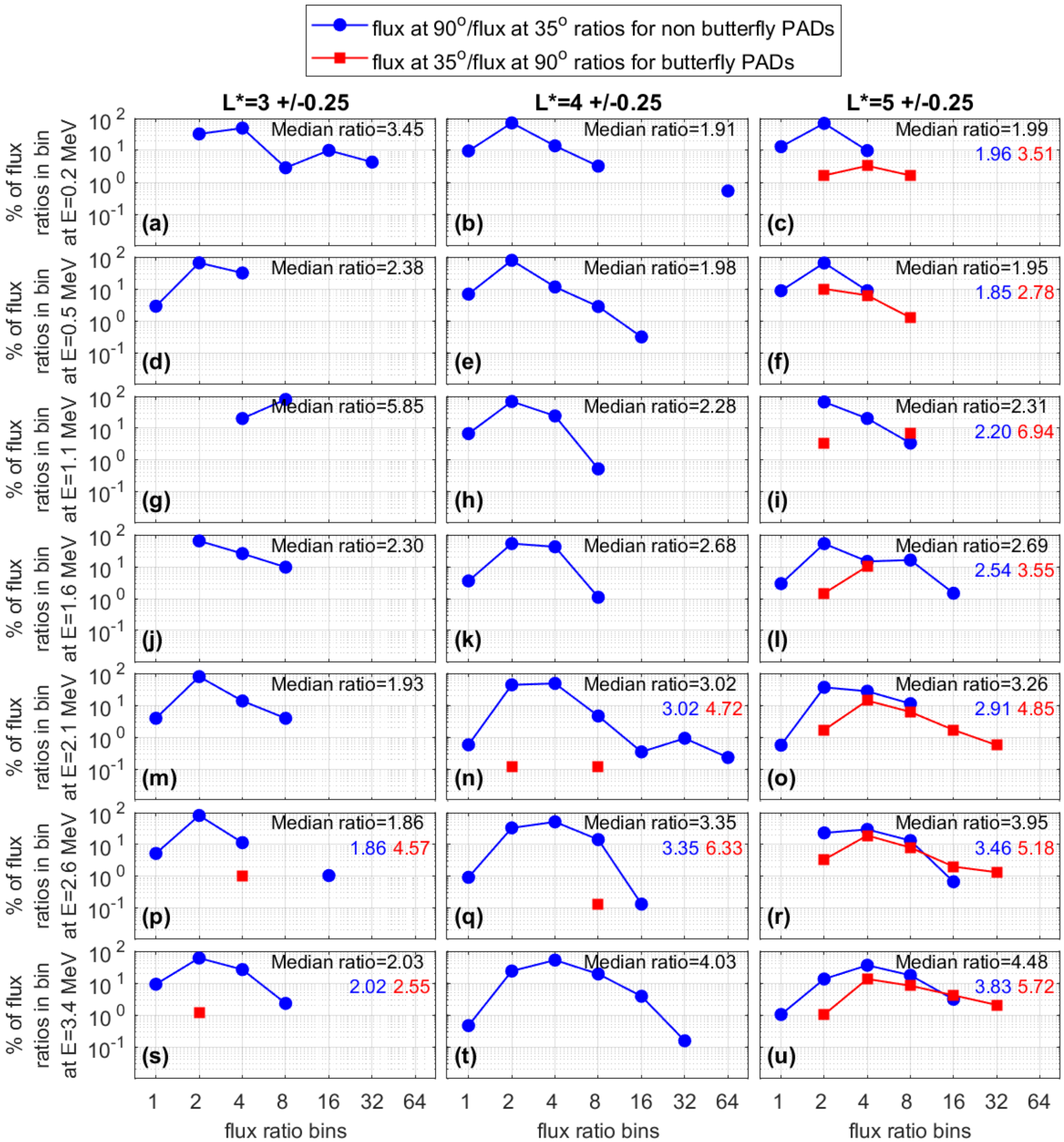

Figure S14. The curves indicate how the flux values at equatorial pitch angles of ~35° and ~90°differ. These results are for Dst=-60 nT ±15 nT, in the same format as the results presented in Figure 9 in the main paper.

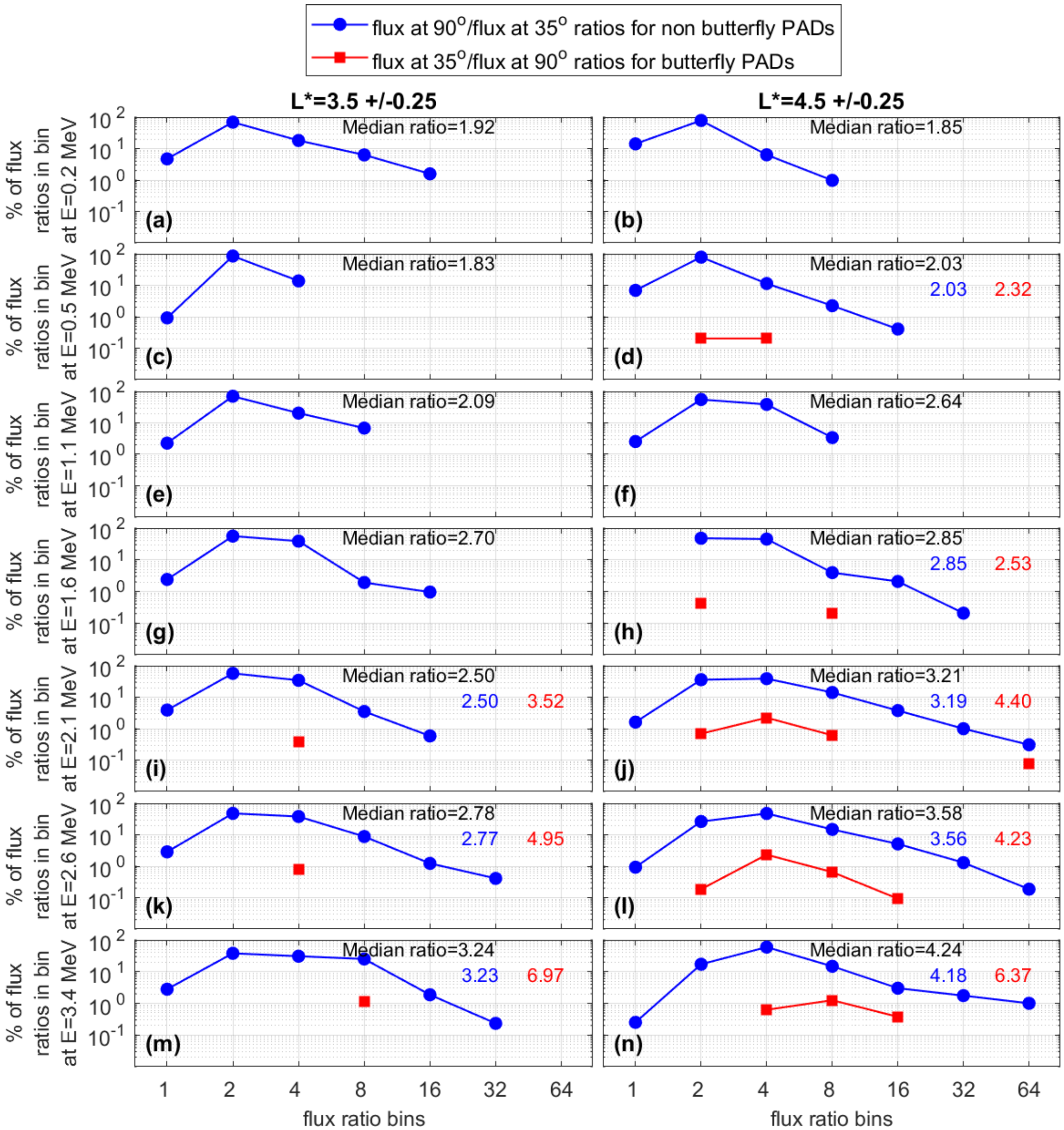

Figure S15. The curves indicate how the flux values at equatorial pitch angles of ~35° and ~90°differ. These results are for Dst=-60 nT ±15 nT at L*=3.5 ±0.25 and L*=4.5 ±0.25 in the same format as the results presented in Figure 9 in the main paper.

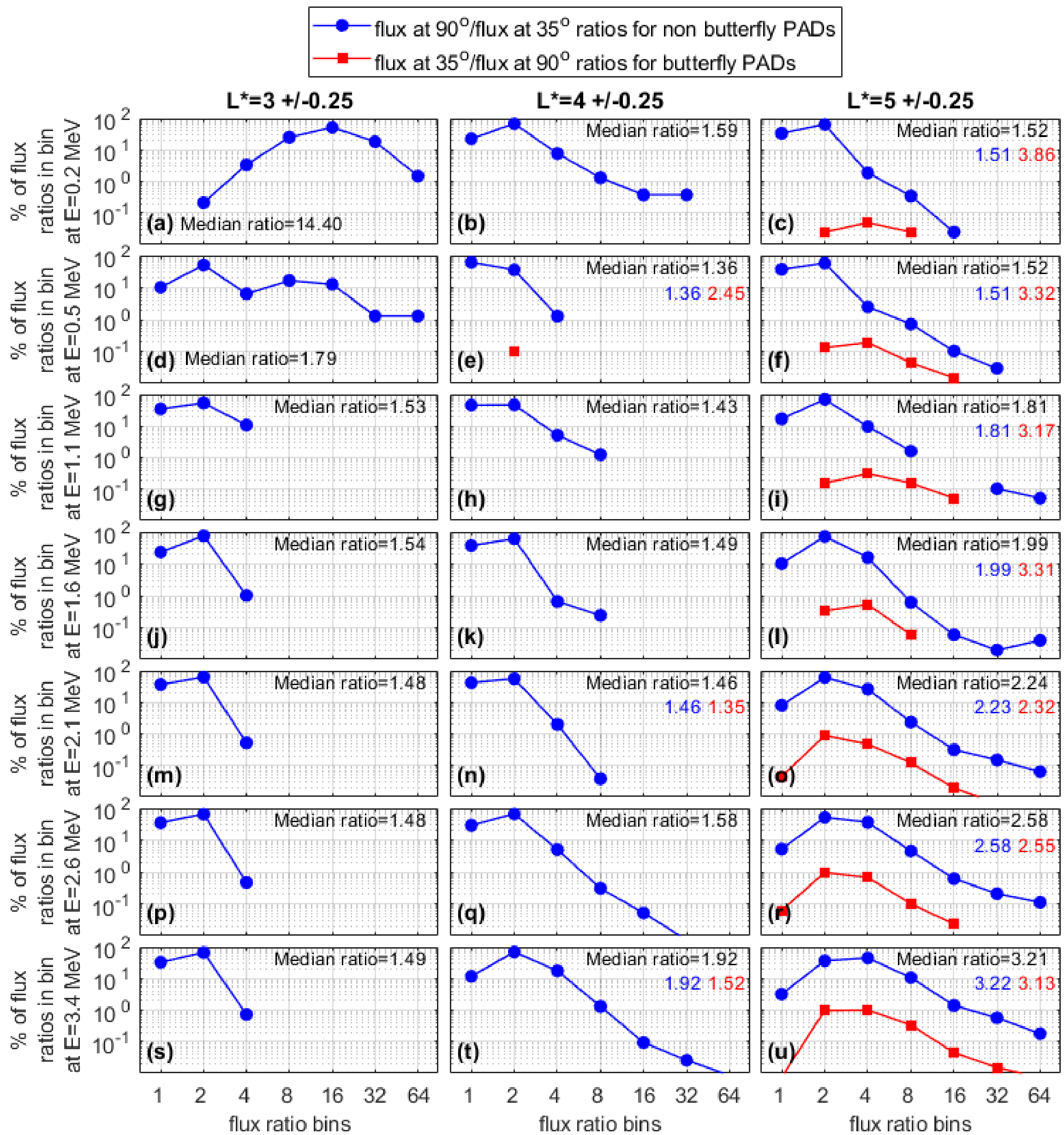

Figure S16. The curves indicate how the flux values at equatorial pitch angles of ~35° and ~90°differ. These results are for Dst=0 nT ±15 nT, in the same format as the results presented in Figure 9 in the main paper.

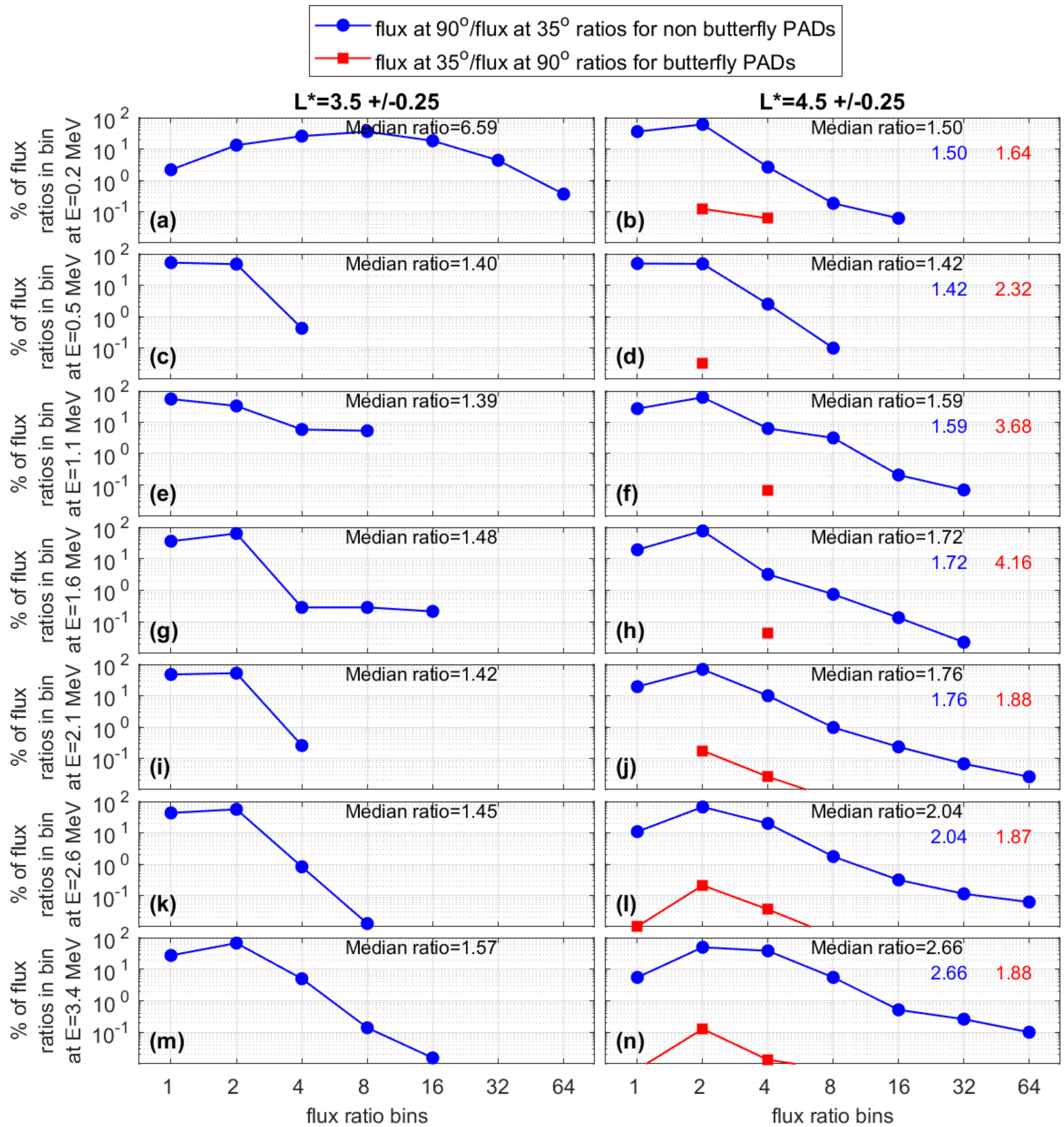

Figure S17. The curves indicate how the flux values at equatorial pitch angles of ~35° and ~90°differ. These results are for Dst=0 nT ±15 nT at L*=3.5 ±0.25 and L*=4.5 ±0.25 in the same format as the results presented in Figure 9 in the main paper.

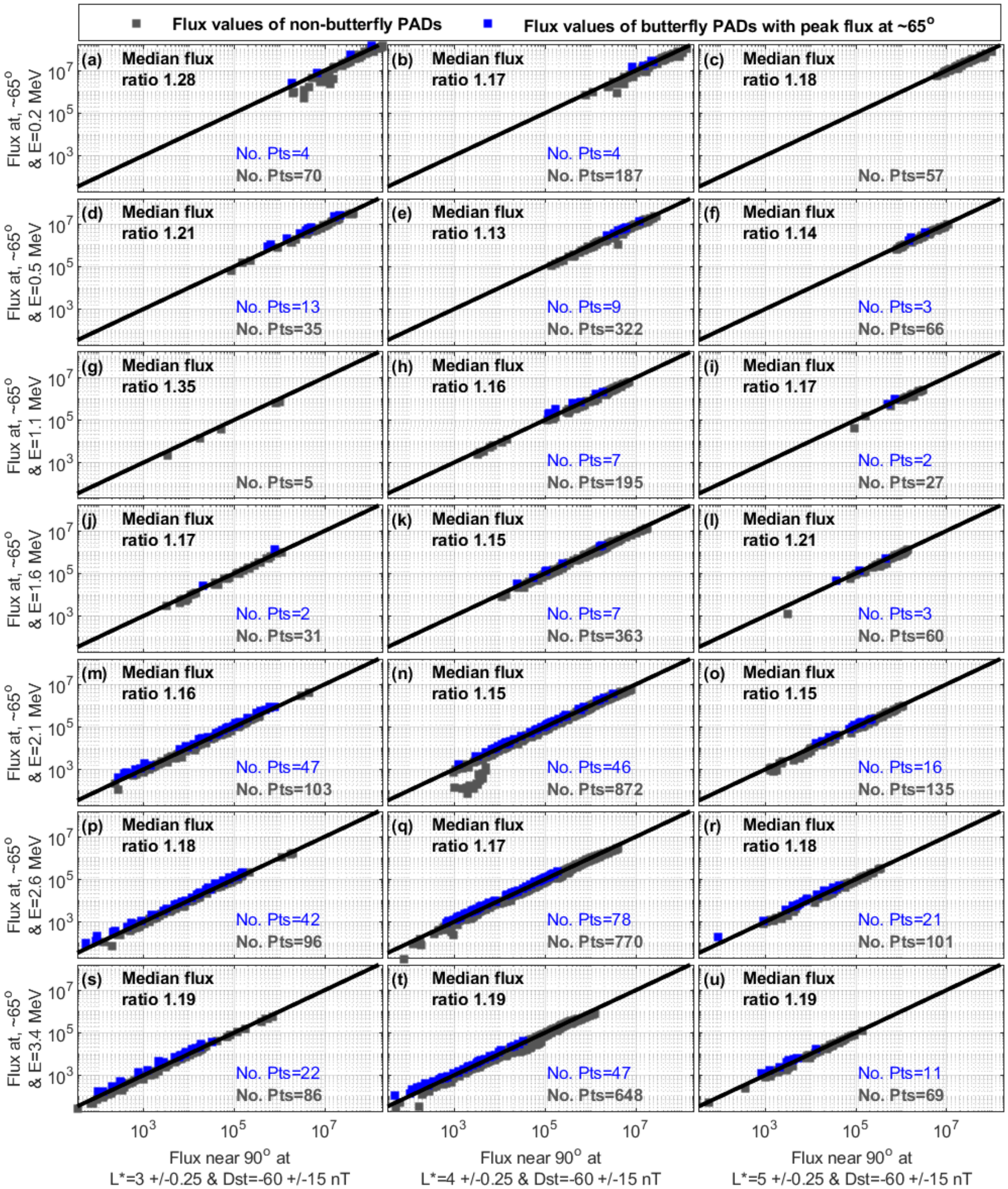

Figure S18. The blue dots indicate results for butterfly PADs that have a peak flux at equatorial pitch angles of 65° ±5°. For these butterfly PADs each data point represents the flux near equatorial pitch angles of 65°, where the flux reaches a peak value, versus the flux near equatorial pitch angles of 90°, where the flux is at a local minimum. Similarly, the gray dots indicate results for non-butterfly PADs. For these non-butterfly PADs each data point represents the flux near an equatorial pitch angle of 90°, where the flux peaks, versus the flux at an equatorial pitch angle of 65°. Results shown here are for Dst=-60 ±15 nT, in a similar format to the results presented in Figure 8 in the main paper.

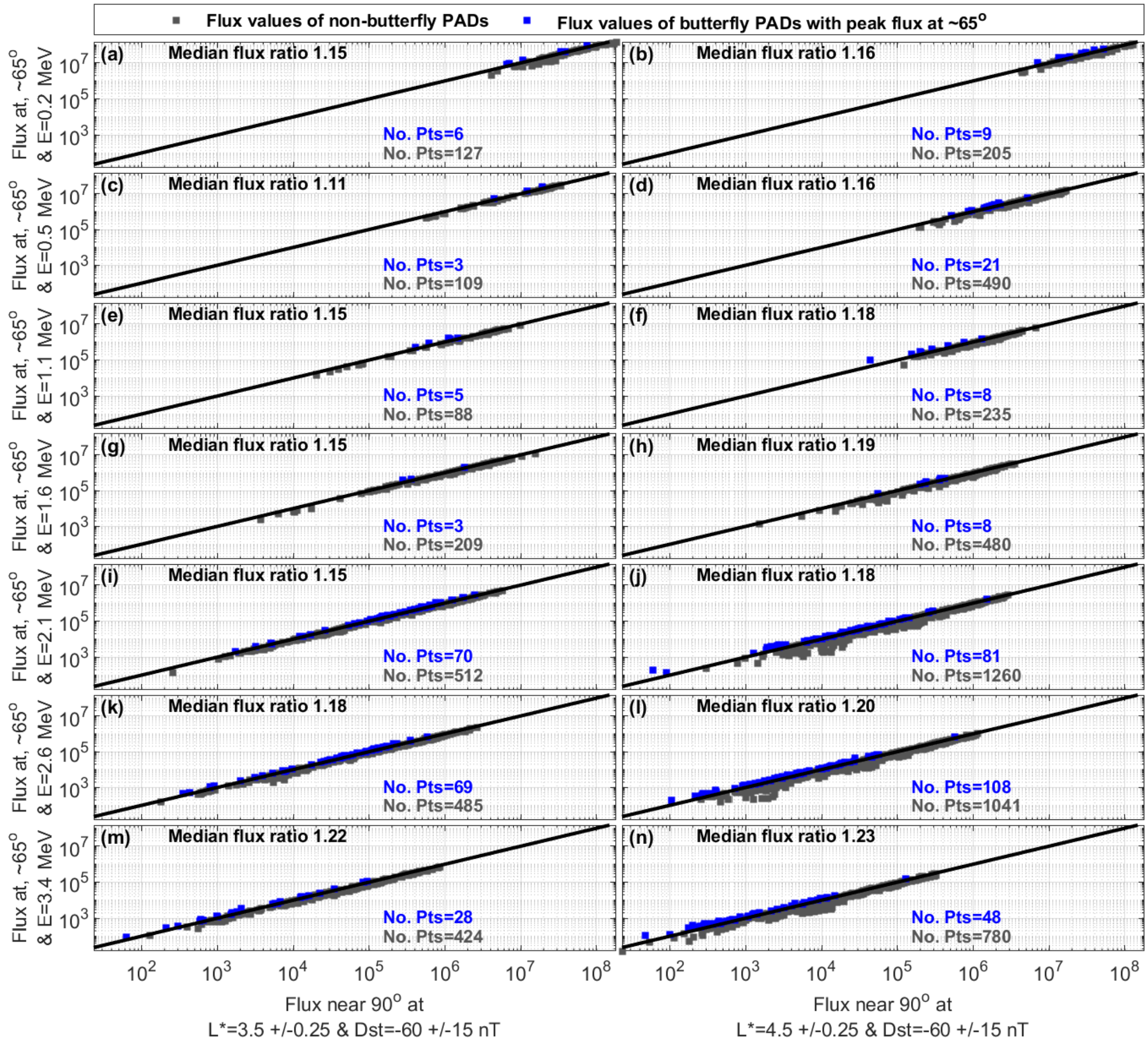

Figure S19. The blue dots indicate results for butterfly PADs that have a peak flux at equatorial pitch angles of 65° ±5°. For these butterfly PADs each data point represents the flux near equatorial pitch angles of 65°, where the flux reaches a peak value, versus the flux near equatorial pitch angles of 90°, where the flux is at a local minimum. Similarly, the gray dots indicate results for non-butterfly PADs. For these non-butterfly PADs each data point represents the flux near an equatorial pitch angle of 90°, where the flux peaks, versus the flux at an equatorial pitch angle of 65°. Results shown here are for Dst=-60 ±15 nT at L*=3.5±0.25 and L*=4.5 ±0.25 in a similar format to the results presented in Figure 8 in the main paper.

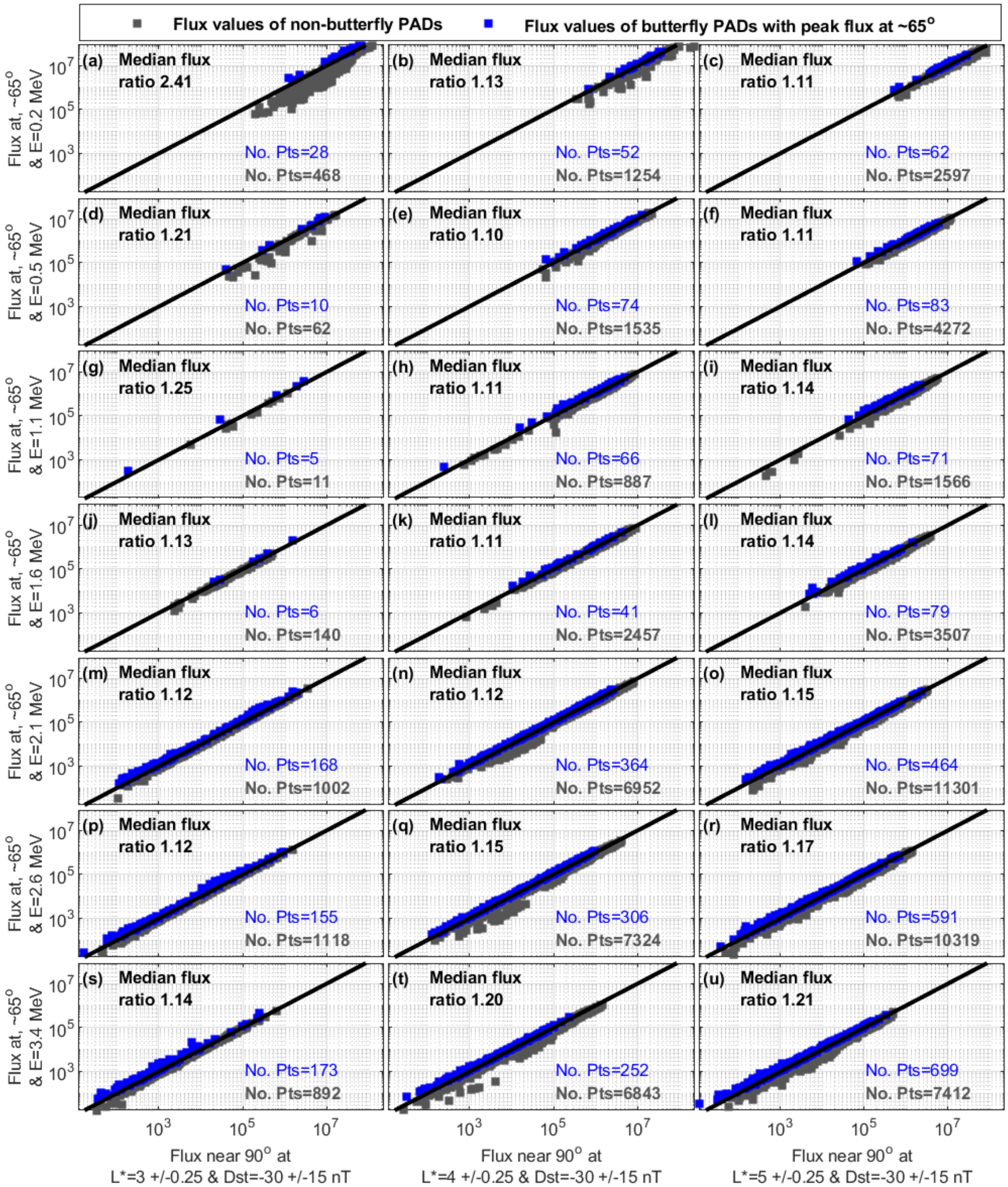

Figure S20. The blue dots indicate results for butterfly PADs that have a peak flux at equatorial pitch angles of 65° ±5°. For these butterfly PADs each data point represents the flux near equatorial pitch angles of 65°, where the flux reaches a peak value, versus the flux near equatorial pitch angles of 90°, where the flux is at a local minimum. Similarly, the gray dots indicate results for non-butterfly PADs. For these non-butterfly PADs each data point represents the flux near an equatorial pitch angle of 90°, where the flux peaks, versus the flux at an equatorial pitch angle of 65°. Results shown here are for Dst=-30 ±15 nT, in a similar format to the results presented in Figure 8 in the main paper.

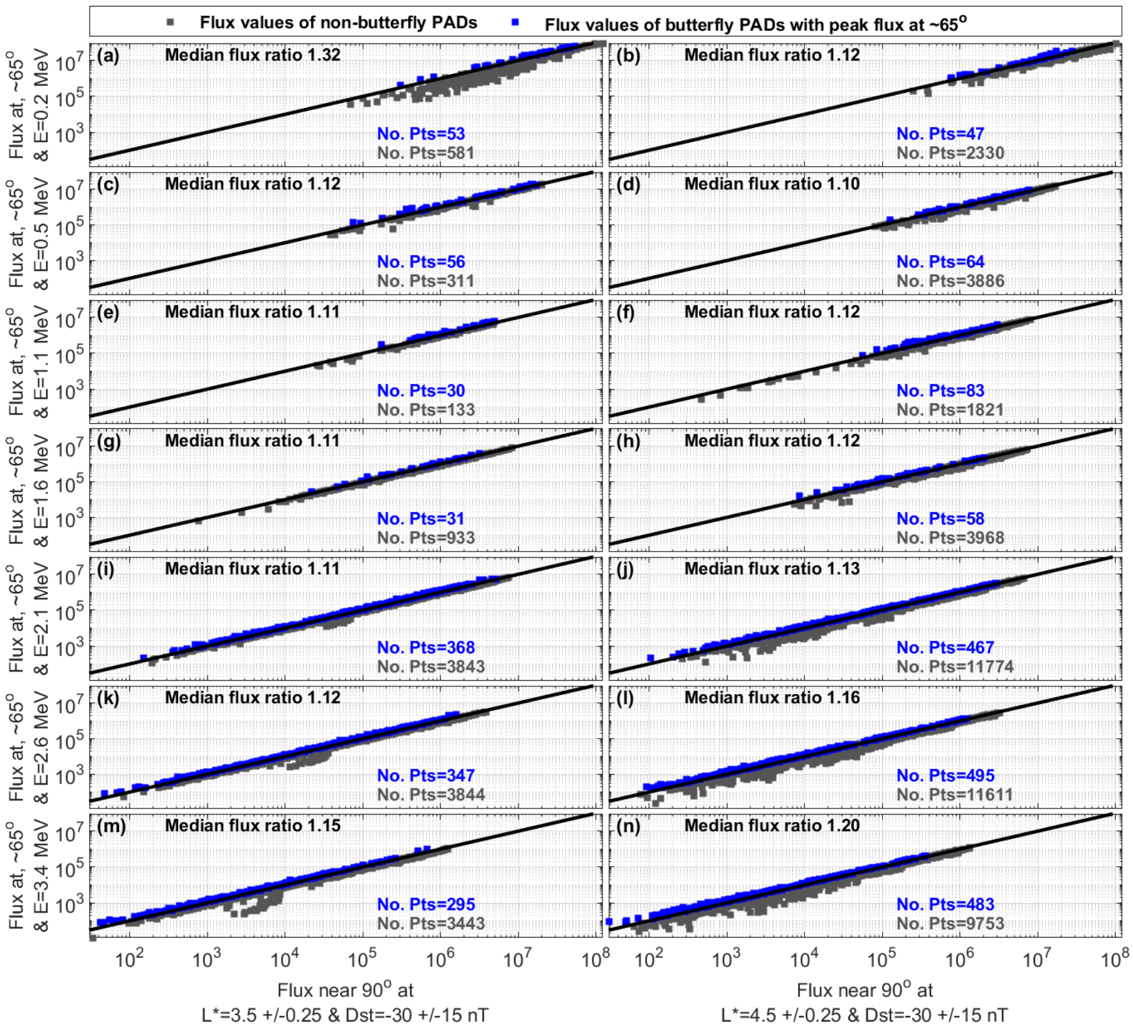

Figure S21. The blue dots indicate results for butterfly PADs that have a peak flux at equatorial pitch angles of 65° ±5°. For these butterfly PADs each data point represents the flux near equatorial pitch angles of 65°, where the flux reaches a peak value, versus the flux near equatorial pitch angles of 90°, where the flux is at a local minimum. Similarly, the gray dots indicate results for non-butterfly PADs. For these non-butterfly PADs each data point represents the flux near an equatorial pitch angle of 90°, where the flux peaks, versus the flux at an equatorial pitch angle of 65°. Results shown here are for Dst=-30 ±15 nT at L*=3.5±0.25 and L*=4.5 ±0.25 in a similar format to the results presented in Figure 8 in the main paper.

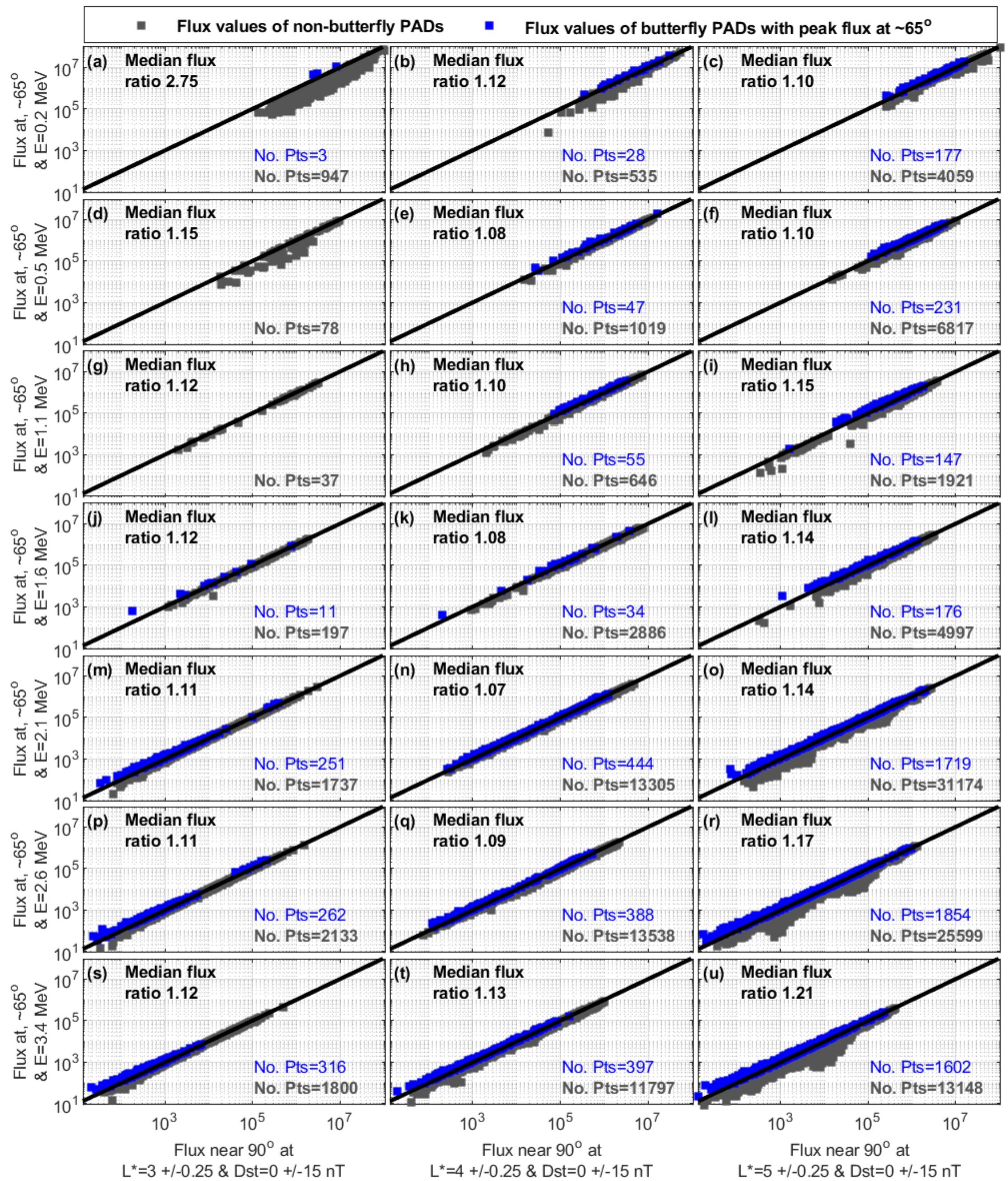

Figure S22. The blue dots indicate results for butterfly PADs that have a peak flux at equatorial pitch angles of 65° $\pm$5°. For these butterfly PADs each data point represents the flux near equatorial pitch angles of 65°, where the flux reaches a peak value, versus the flux near equatorial pitch angles of 90°, where the flux is at a local minimum. Similarly, the gray dots indicate results for non-butterfly PADs. For these non-butterfly PADs each data point represents the flux near an equatorial pitch angle of 90°, where the flux peaks, versus the flux at an equatorial pitch angle of 65°. Results shown here are for Dst=0 ±15 nT, in a similar format to the results presented in Figure 8 in the main paper.

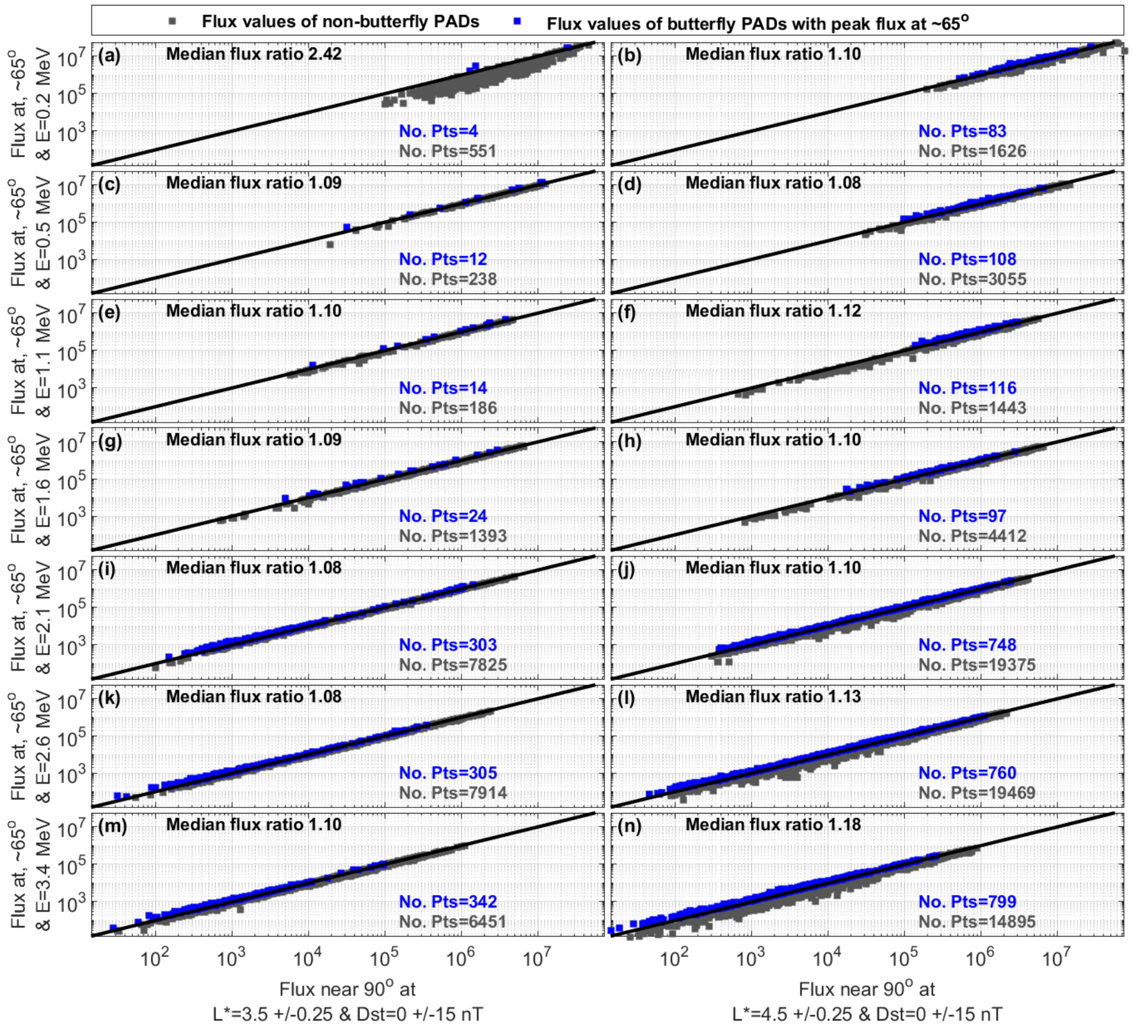

Figure S23. The blue dots indicate results for butterfly PADs that have a peak flux at equatorial pitch angles of 65° ±5°. For these butterfly PADs each data point represents the flux near equatorial pitch angles of 65°, where the flux reaches a peak value, versus the flux near equatorial pitch angles of 90°, where the flux is at a local minimum. Similarly, the gray dots indicate results for non-butterfly PADs. For these non-butterfly PADs each data point represents the flux near an equatorial pitch angle of 90°, where the flux peaks, versus the flux at an equatorial pitch angle of 65°. Results shown here are for Dst=0 ±15 nT at L*=3.5±0.25 and L*=4.5 ±0.25 in a similar format to the results presented in Figure 8 in the main paper.

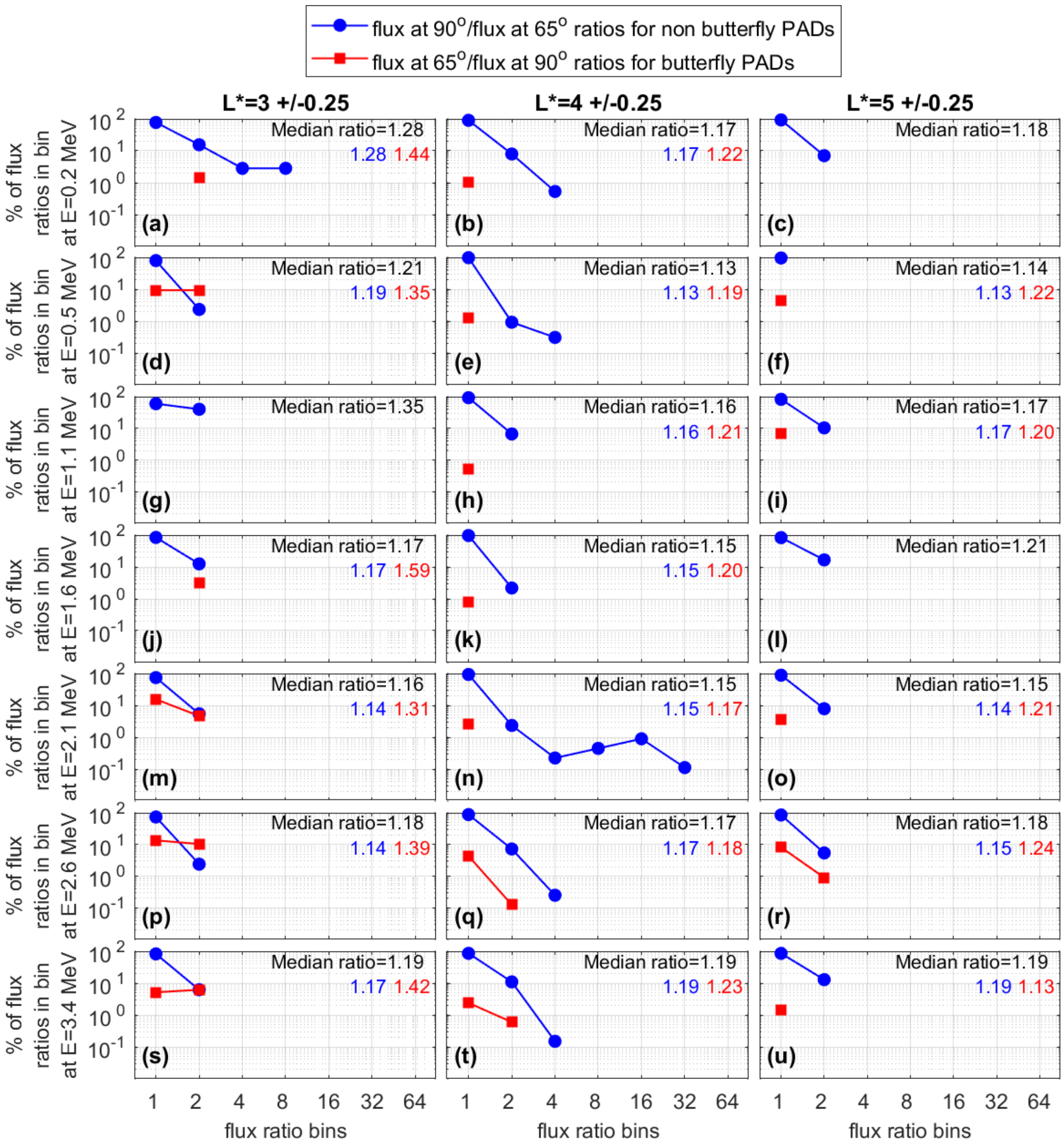

Figure S24. The curves indicate how the flux values at equatorial pitch angles of ~65° and ~90°differ. These results are for Dst=-60 nT ±15 nT, in the same format as the results presented in Figure 9 in the main paper.

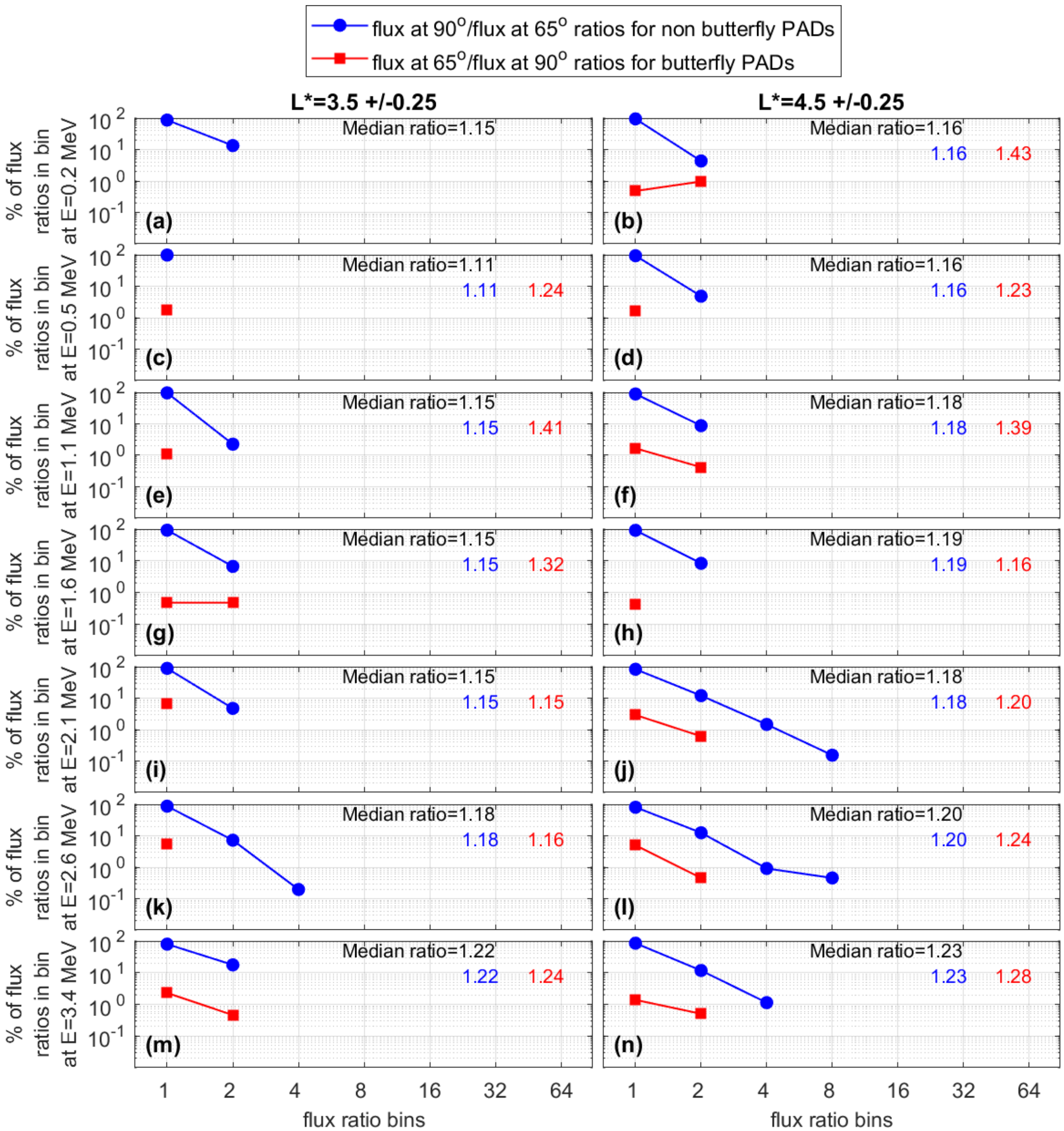

Figure S25. The curves indicate how the flux values at equatorial pitch angles of ~65° and ~90°differ. These results are for Dst=-60 nT ±15 nT at L*=3.5 ±0.25 and L*=4.5 ±0.25 in the same format as the results presented in Figure 9 in the main paper.

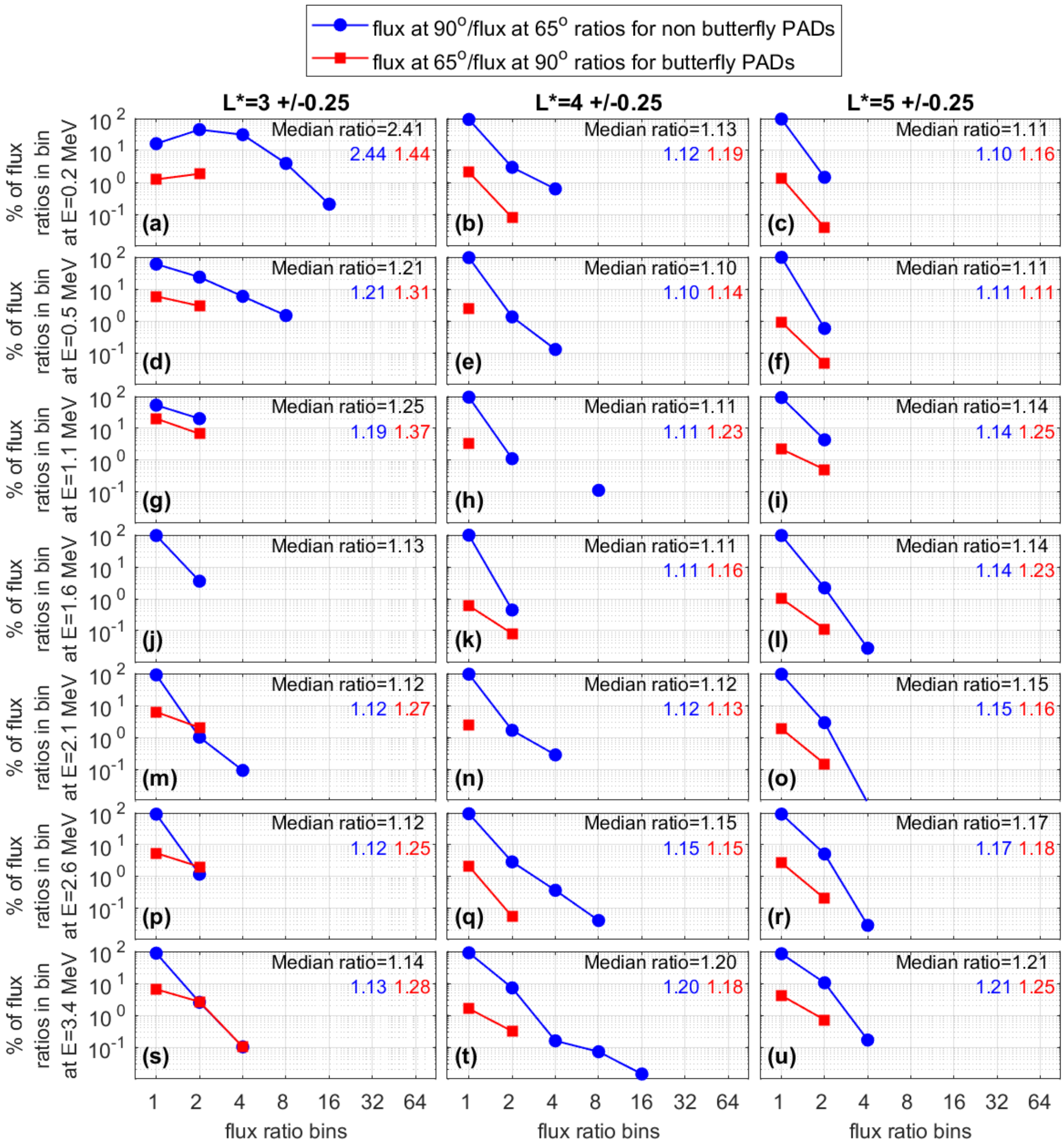

Figure S26. The curves indicate how the flux values at equatorial pitch angles of ~65° and ~90°differ. These results are for Dst=-30 nT ±15 nT, in the same format as the results presented in Figure 9 in the main paper.

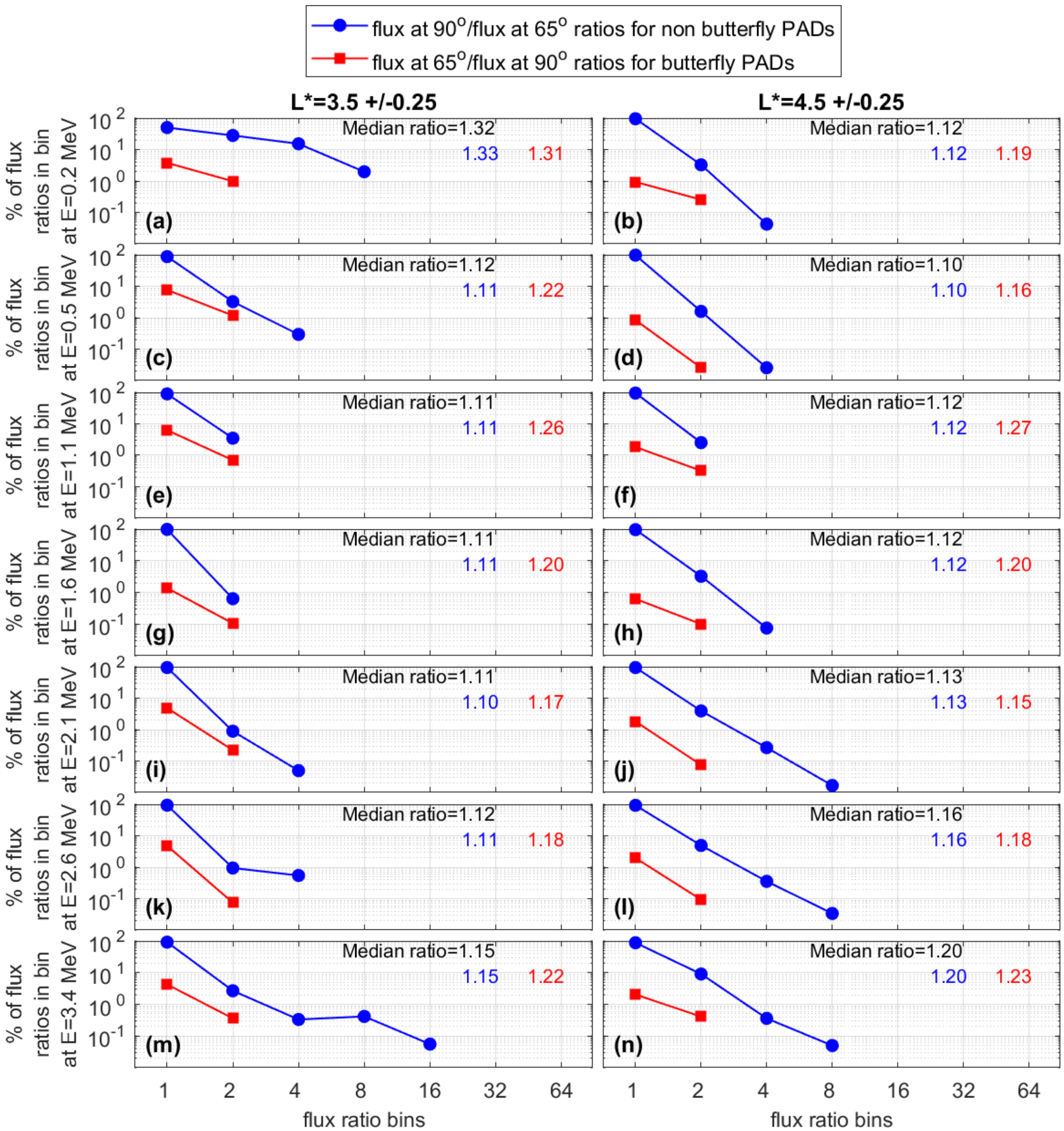

Figure S27. The curves indicate how the flux values at equatorial pitch angles of ~65° and ~90°differ. These results are for Dst=-30 nT ±15 nT at L*=3.5 ±0.25 and L*=4.5 ±0.25 in the same format as the results presented in Figure 9 in the main paper.

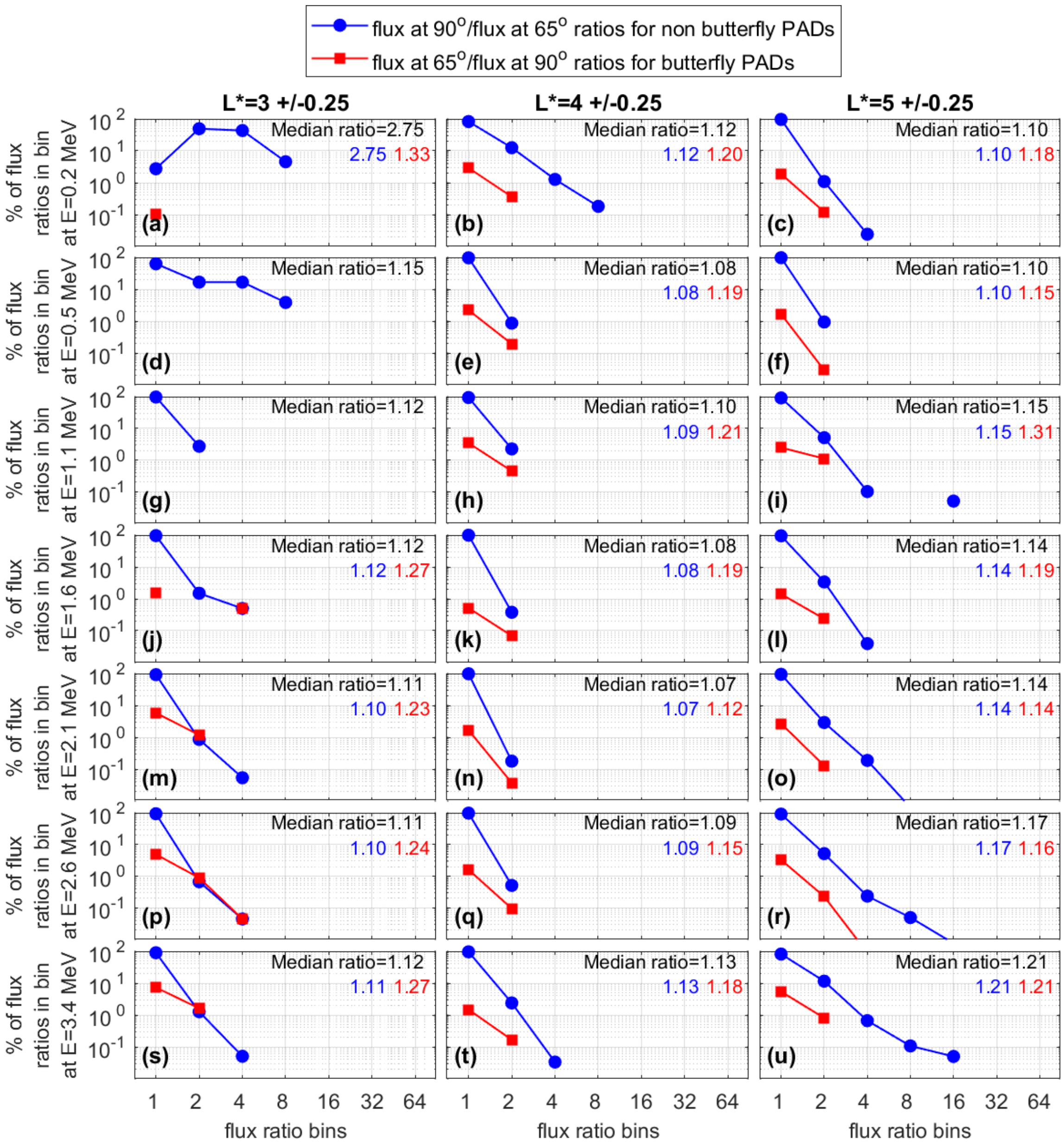

Figure S28. The curves indicate how the flux values at equatorial pitch angles of ~65° and ~90°differ. These results are for Dst=0 nT ±15 nT, in the same format as the results presented in Figure 9 in the main paper.

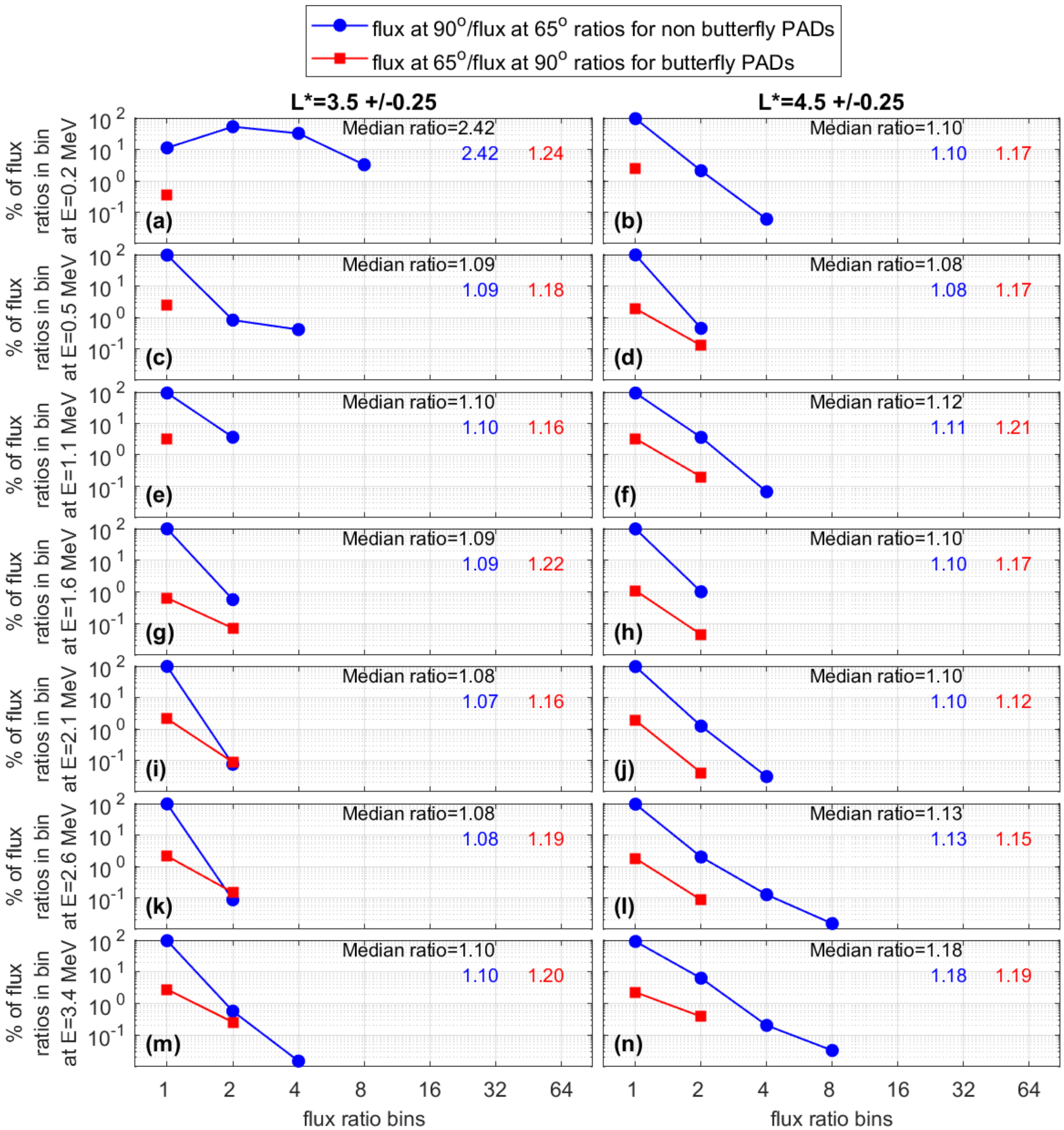

Figure S29. The curves indicate how the flux values at equatorial pitch angles of ~65° and ~90°differ. These results are for Dst=0 nT ±15 nT at L*=3.5 ±0.25 and L*=4.5 ±0.25 in the same format as the results presented in Figure 9 in the main paper.